Electronic, magnetic and transport properties of rare-earth monopnictides

Electronic, magnetic and transport properties of rare-earth monopnictides

Chun-Gang Duan[1,2]**, R F Sabirianov**[2,3]**, W N Mei**[2,3]**, P A Dowben**[1,2]**, S S Jaswal**[1,2] **and E Y Tsymbal**[1,2]

[1] Department of Physics, University of Nebraska-Lincoln, Lincoln, NE 68588, USA
[2] Nebraska Center for Materials and Nanoscience, University of Nebraska-Lincoln, Lincoln, NE 68588, USA
[3] Department of Physics, University of Nebraska at Omaha, Omaha, NE 68182, USA

E-mail: wxbdcg@gmail.com

Abstract

The electronic structures and magnetic properties of many rare-earth monopnictides are reviewed in this article. Possible candidate materials for spintronics devices from the rare-earth monopnictide family, i.e. high polarization (nominally half-metallic) ferromagnets and antiferromagnets, are identified. We attempt to provide a unified picture of the electronic properties of these strongly correlated systems. The relative merits of several *ab initio* theoretical methods, useful in the study of the rare-earth monopnictides, are discussed. We present our current understanding of the possible half-metallicity, semiconductor–metal transitions, and magnetic orderings in the rare-earth monopnictides. Finally, we propose some potential strategies to improve the magnetic and electronic properties of these candidate materials for spintronics devices.

(Some figures in this article are in colour only in the electronic version)

Contents

1. Introduction

Half-metallic ferromagnets, which were first so named by de Groot *et al* in 1983 [1], have attracted interest from both experimentalists and theorists [2, 3]. Currently, most of the nominally half-metallic ferromagnets found are compounds that involve transition metal elements, for example CrO_2, Fe_3O_4, Co_2MnSi [3], and they suffer from a number of deficiencies that limit their application as high polarization materials in spintronics. The electronic structures of nominally half-metallic systems are, nonetheless of considerable interest as an avenue for studying the interplay between high polarization and band structure. Their attraction remains in spite of the growing recognition that true half-metallic character is unlikely to be ever demonstrated at finite temperatures, due to magnons [4, 5], as well as zero-temperature interactions [6, 7]. It is natural, therefore, to explore the rare-earth compounds, as rare-earth elements generally have much larger magnetic moments and demonstrate some fascinating phenomena [8, 9].

Rare-earth elements are chemically very similar due to an almost identical outer electron arrangement [10]. It remains, however, difficult to obtain impurity-free single crystals of the rare-earths or rare-earth compounds, and this may be responsible for some of the long-standing controversies concerning their electronic structure, transport properties and magnetic properties.

The rare-earths do, however, have different occupation numbers for the shallow inner 4f shell, ranging from 0 to 14 through the series La to Lu. This changing 4f occupation means that the rare-earth elements and their compounds have a wide range of different magnetic properties and electronic structures. Due to the unfilled 4f shells of rare-earth atoms, it is a challenging problem to obtain an accurate theoretical description of the electronic structure of rare-earth compounds [11]. In spite of the fact that the 4f energy levels often overlap with the non-4f broad bands of the system, they generally form very narrow resonances, and are often treated as core states in the theoretical efforts. Due to the highly localized nature of the 4f electrons, the direct f–f interactions between neighbouring rare-earth atoms are generally considered to be nearly negligible. However, there is evidence that this general belief has to be modified. For instance, in the cases of cerium (uranium) compounds [12–16], 4f (5f) level dispersion was observed experimentally, suggesting smaller f level localization in these systems. The unoccupied f states certainly will adopt all the trappings of band structure in every conventional sense.

f orbital moments generally cannot be quenched by the crystal field. Therefore the total magnetic moments have both orbital and spin components, and spin–orbital interactions are particularly strong for many of the rare-earth elements and compounds. These inner shell magnetic moments are largely aligned through intra-atomic s(d)–f exchange interaction and weaker inter-atomic s–s (d–d) exchange interactions; thus the rare earth pnictide magnetic transition temperatures are generally much lower than those of 3d transition metal elements or compounds. In spite of the increasingly compelling evidence for band structure [12], the 4f bands are generally very narrow, significantly different from the bands dominated by s, p and d states. Therefore there exist strong on-site Coulomb repulsions between the highly localized f electrons [17, 18]. This makes the independent particle approximation no longer valid and calculations based on local spin density approximation (LSDA) fail to describe the rare-earth 4f electrons correctly. To explain the behaviours of rare-earth 4f electrons, many-body effects must be taken into account and more accurate approximations or calculations beyond LSDA are absolutely necessary.

With the availability of better quality single crystals and thin films, together with the tremendous theoretical efforts in combining many-body theory and density functional theory (DFT) in the last 20 years, a better picture of electronic structure and magnetic properties of rare-earth elements and their compounds has taken shape. It is the major objective of this review to provide a detailed account of the progress made in the field of rare-earth monopnictides, RX (X = N, P, As, Sb, Bi). This particular family is chosen because there are more than 50 members that crystallize in the simple NaCl-type structure, making the rare-earth monopnictides excellent candidates for both experimental and theoretical analysis.

In providing an overview of the electronic, magnetic and transport properties of rare-earth monopnictides, we have given some preference to GdN and EuN. GdN and EuN are considered to be the most promising nominally halfmetallic ferromagnets in the RX family. Attracting our attention are the mechanisms for magnetic ordering, the pressure/strain and impurity effects.

2. Early experiments and theoretical studies

Studies of the rare-earth elements and their compounds can be traced back more than 70 years. The agreement between experiment and calculations made by Van Vleck and Frank [19] on the effective magneton number of the rare-earth ions was regarded as one of the most successful applications of quantum mechanics to magnetism [20]. The surge in the study of rare-earth compounds in the 1960s was mainly motivated by a search for new ferromagnetic semiconductors [21–27]. Researchers began realizing that it was too complicated to interpret the experimental results if crystal distortions or impurities were considered. Thus, investigations on rare-earth monopnictides gradually became one of the most important directions in the study of rare-earth compounds, mostly because these binary compounds crystallize into the simple NaCl-type structure and were supposed to be more amenable to theoretical analyses [21].

Nevertheless, even with such a simple structure, the full understanding of rare-earth monopnictides' electronic structure and magnetic properties is still not complete. Rare-earth monopnictides demonstrate rich magnetic orderings and their electronic structures are sensitive to external pressure and impurities. Due to the poor computational power and limited theoretical methods, earlier theoretical studies were restricted to analytical model calculations, such as crystalline field [23], effective-point-charge [28], d–f Coulomb interaction [29] and p–f mixing [30]. These calculations could explain some phenomena for certain rare-earth monopnictides, but the overall agreement with experiments for the whole RX family was not satisfactory.

The earliest *ab initio* band structure calculation of the rare-earth monopnictides was carried out by Hasegawa and Yanase in 1977 [31]. They adopted an augmented planewave method with Slater $X\alpha$ exchange potential [32] to calculate the energy bands of GdX (X = N, P, As, Sb), in a self-consistent way. To deal with the 4f electrons, they used the frozen-core approximation, i.e. the 4f electrons are treated as core electrons. On the basis of their calculations, Hasegawa and Yanase claimed that GdN is a semiconductor with an adjusted band gap of 1 eV, and other Gd monopnictides are semimetallic. But they also realized that if spin polarization is taken into account, then the 5d–4f exchange splitting, which was estimated also to be around 1 eV, could make GdN exhibit metallic character as well [31].

In 1988, using a tight-binding model with parameters chosen to fit the band structures calculated by Hasegawa and Yanase [31], Narita studied the magnetic susceptibilities and spin structures of GdX [33]. This was the first attempt to understand the magnetic properties of rare-earth monopnictides from band structure calculations, though Narita obtained wrong magnetic ground states for these compounds. Using a similar method, Xia *et al* [34] studied the electronic structure of the GdAs/GaAs superlattice in 1991.

The first spin-polarized *ab initio* calculations on rare-earth monopnictides was provided by Petukhov *et al* in 1994 [35]. Using the linear-muffin-tin-orbital (LMTO) method within LSDA and treating the Er 4f states as localized corelike states with fixed spin occupancies, Petukhov and coworkers calculated the electronic structure of ErAs and $Er_xSc_{1-x}As$ alloys. Later, in 1996, they studied extensively the electronic structures, equilibrium lattice constants, cohesive energies, bulk moduli and magnetic moments of GdX and ErX (X = N, P, As) [36]. They found that the corelike treatment is satisfactory for most purposes not involving the 4f electrons directly. They also found that the electron band exchange splittings of the nitrides are significantly larger than those for the arsenides and phosphides, rendering GdN metallic for one spin channel and semiconducting for the other. Thus, Petukhov, Lambrecht and Segall were actually the first to claim that GdN could be half-metallic, within their calculation scheme, which did not involve the 4f states explicitly. There have been other theoretical studies on Gd compounds; for example, Kasuya and Li tried f–d mixing and f–d exchange interactions to explain the strong ferromagnetism in GdN in 1997 [37].

The early experimental reports on rare-earth monopnictides are widely scattered in the literature. For reviews on experimental studies before 1970s, one can refer to [25, 38] and [39], but focusing on the experimental studies on the electronic, transport and magnetic properties, in the period from 1970s to 1990s, provides an insight into the parallel growth of materials science and electron spectroscopy. In the rare-earth monopnictide family, the Gd monopnictides have been extensively investigated. This is because Gd is located in the middle of the rare-earth group in the periodical table, and the Gd 4f orbitals are exactly half occupied; hence the orbital angular momentum is zero, as the ground state of Gd^{3+} is $^8S_{7/2}$. Thus the spin–orbit, multipole, p–f and d–f mixing interactions are small [33], greatly simplifying the problems associated with electronic structure. In addition, the Gd monopnictides (and Gd metal) generally have much higher transition temperatures, which is also attractive in many respects [38].

Kaldis reported the first successful growth of large single crystals of GdP in 1974 [40]. This opened the door to a reliable determination of the electronic structure of GdP. Based on optical investigation [41], Güntherodt *et al* deduced that the crystal-field splitting of the Gd 5d states is about 1.8 eV and the positions of occupied Gd 4f levels in GdP are about 7 eV below E_F. They also found that GdP exhibits metal-like conductivity. Later experiments on GdN were controversial: GdN was reported as a semiconductor [42] and a semimetal [43]. Studies on the magnetic exchange interaction on Gd compounds clearly demonstrated that the free carriers contribute to a Ruderman–Kittel–Kasuya–Yosida (RKKY) [44–46] indirect exchange interaction [47, 48].

Urban *et al* [49] observed a large variation of the thermal broadening of the electron spin resonance (ESR) linewidth of Gd across the pnictides in 1978. They claimed that the conduction electrons exhibit almost d character; thus the exchange interaction depends on the amount of overlapping between d wave functions. Palmstrøm *et al* [50] successfully grew single-crystal ErAs films on GaAs in 1988. Later magneto-transport measurements showed that ErAs is a low-density semimetal that magnetically orders at low temperature (4.5–4.8 K) [51].

In 1990, Degiorgi *et al* reported on results obtained from large single crystals of cubic and stoichiometric YbN [52]. They claimed that YbN is a self-compensated semimetal with the occupied f states about 6 eV below E_F and the empty f states about 0.2 eV above E_F. Their later studies confirmed the semimetallic nature of YbP and YbAs [53]. Chattopadhyay *et al* carried out high-pressure magnetization and neutron-diffraction experiments on CeSb in 1994 [54]. They found that the magnetic ordering of CeSb is very sensitive to hydrostatic pressure. Waldfried *et al* used angle-resolved photoemission to study the electronic structure of dissociatively chemisorbed nitrogen on Gd(0001) in 1995 [55]. Xiao and Chien found that GdN films are insulating [56]. Li *et al* reported the growth of large single crystals of GdX (X = P, As, Sb, Bi) in 1996 and found them all to be well-compensated semimetals that order antiferromagnetically [57, 58]. The photoemission studies of Yamada *et al* showed that the occupied 4f states in GdP lie around 8.4 eV below E_F, and shift down from GdP to GdBi [59]. The experiments on polycrystal GdN confirmed that stoichiometric GdN is ferromagnetic with a transition temperature 58 K [60].

3. Recent theoretical and experimental progresses

Recent theoretical progress in the rare-earth monopnictide studies follows the development of electronic structure calculations in solids. For strongly correlated systems, the accurate evaluations require going beyond the LSDA scheme. The following methods have been developed to overcome the deficiency of LSDA calculations.

3.1. Self interaction correction (SIC)

Despite its impressive successes [61], LSDA has an intrinsic deficiency, i.e. the self-interaction energy problem [62]. The self-Coulomb and self-exchange interactions in LSDA do not cancel completely, as in the case of Hartree–Fock approximation. This means that the LSDA will fail to correctly describe systems with strong electron–electron interactions. Numerous efforts have been made to address this problem [62–65]. In the self-interaction-corrected local-spin density approximation (SIC–LSDA) [65], the non-physical electron self-interactions, including both SIC Coulomb and corresponding SIC exchange–correlation terms, are subtracted from the LSDA Hamiltonian, and the energy functional is written as

$$E_{SIC} = E_{LSDA} - \sum_i^{occ} \left(\int \frac{n_i(\mathbf{r})n_i(\mathbf{r}')}{|\mathbf{r}-\mathbf{r}'|} \, \mathrm{d}^3r \, \mathrm{d}^3r' + \int n_i(\mathbf{r})\varepsilon_{xc}(n_i(\mathbf{r}), 0) \, \mathrm{d}^3r \right), \tag{1}$$

where E_{LSDA} is the energy functional in the LSDA, $n_i(\mathbf{r})$ is the charge density corresponding to the ith solution of the SIC–LSDA equation, and $\varepsilon_{xc}(n_\uparrow, n_\downarrow)$ is the exchange–correlation energy density of a homogeneous system with spin densities $n_\uparrow$ and $n_\downarrow$. The SIC approach generates an orbital-dependent potential which can be significant for localized states, yielding a much-improved description of the static Coulomb correlation effect compared to that provided by the LSDA. The applications of SIC–LSDA are often quite successful [66–69].

Another advantage of the SIC–LSDA method is that the minimization of total energy, with respect to the number of localized electrons, leads to a determination of the nominal *valence*

defined as the integer number of electrons available for band formation

$$N_{\mathrm{v}} = Z - N_{\mathrm{core}} - N_{\mathrm{SIC}},\tag{2}$$

where Z is the atomic number, and N_{core} and N_{SIC} are the number of core and localized (SIC) electron states, respectively. This information is important for the analyses of chemical properties of rare-earth compounds [67].

Application of the SIC–LSDA methodology to the rare-earth monopnictides was carried out by Aerts *et al* [70], Horne *et al* [71], and Szotek *et al* [72] in 2004. Together, these studies represent a systematic study of the electronic structure of 13 rare-earth nitrides, from CeN to YbN. The calculations show that the rare-earths are trivalent in the mono-nitride ground state, with the exception of Ce, which is tetravalent in CeN. On the basis of the SIC–LSDA calculations, the claim is that these rare-earth nitrides display a wide range of electronic properties, despite having the same structure and similar lattice constants. Specifically, TbN, DyN and HoN are found to be narrow gap insulators, and CeN, ErN, TmN and YbN are metallic in both spin channels, while PrN, NdN, PmN, SmN, EuN and GdN are half-metallic ferromagnets in these ground-state calculations. The f-band manifold is split by the SIC into localized and bandlike f electrons. Because of the different degree of hybridization between the rare-earth bandlike f and the nitrogen p states, in the vicinity of the Fermi level, these compounds demonstrate different electronic properties. This is consistent with the electronic structures of SmX (X = N, P, As, Sb, Bi) which have been studied by Svane *et al* [73]. Svane and co-workers found that the occupied f bands are formed in the vicinity of the Fermi level in all the SmX compounds.

3.2. LSDA + U

In the LSDA, the potential is treated as an averaged orbital-independent one-electron potential. This may be a reasonable approximation for weakly correlated system, which corresponds to an extreme case of a Hubbard model [74] where the on-site Coulomb repulsion (Hubbard U) approaches zero. For strongly correlated systems like Mott insulators, however, ignoring the effective Coulomb parameter U results in an incorrect prediction of the energy gap. The LSDA + U [75–78] method was initially proposed to describe Mott insulators correctly. Following the Anderson model [79], electrons are separated into two subsystems: localized d or f electrons and delocalized s or p electrons. The d–d (f–f) interaction is described by the Hubbard term $\frac{1}{2}U \sum_{i \neq j} n_i n_j$, where n_i is the d(f)-orbital occupancy, instead of the LSDA averaged term (approximately) $E = UN(N-1)/2$. Then a new energy functional can be written as

$$E^{\mathrm{LSDA}+U} = E^{\mathrm{LSDA}} - \tfrac{1}{2}UN(N-1) + \tfrac{1}{2}U \sum_{i \neq j} n_i n_j,\tag{3}$$

and the orbital energies ε_i are given by

$$\varepsilon_i^{\mathrm{LSDA}+U} = \frac{\partial E^{\mathrm{LSDA}+U}}{\partial n_i} = \varepsilon_i^{\mathrm{LSDA}} + U(\tfrac{1}{2} - n_i).\tag{4}$$

This new formulation splits the orbital energies of occupied localized electrons ($n_i = 1$) and unoccupied localized electrons ($n_i = 0$) by U, thus reproducing the qualitatively correct physics for Mott–Hubbard insulators [77]. The above analysis is, however, only a simplified overview. The realization of the LSDA+U scheme, in practice, requires much more theoretical effort [75] which is not addressed here. In passing, it is worth noting that a rotationally invariant form of the LSDA + U functional is given by

$$E^{\mathrm{LSDA}+U} = E^{\mathrm{LSDA}} + \frac{U - J}{2} \sum_{\sigma} [\mathrm{Tr}\,\rho^{\sigma} - \mathrm{Tr}(\rho^{\sigma} \rho^{\sigma})],\tag{5}$$

in which σ is the spin, and U and J are the (spherically averaged) screened Coulomb electron–electron interaction (Hubbard parameter U) and Hund's rule exchange parameter (Stoner parameter I), respectively [80].

In practice, parameters U and J can be taken as adjustable parameters (for example, obtained through comparison with photoemission and inverse photoemission experiments). U and J can also be evaluated from the LSDA through the supercell LSDA approach [81]. Specifically, $U = F^0$, $J = (F^2 + F^4)/14$ for d electrons, and $J = (286F^2 + 195F^4 + 250F^6)/6435$ for f electrons [78], where F^k ($k = 0, 2, 4, 6$) are Slater integrals [82].

The first LSDA $+ U$ calculation on the rare-earth monopnictides was carried out by Liechtenstein *et al* [83] in 1994. They studied the electronic structure and magneto-optical effects in CeSb. The Ce 4f level is found to be 2 eV below the Fermi level and is hybridized with Sb p bands. Using the LMTO method, in 2003 Komesu *et al* [84] studied the electronic structure of ErAs and obtained band dispersions qualitatively similar with experiment. In 2004, Duan *et al* [85] considered the spin–orbit coupling in the LSDA $+ U$ calculation of bulk ErAs, using the full-potential linear-augmented-plane-wave (FLAPW) method [86]. The theoretical 4f multiplet structure agrees well with photoemission experiments. In addition, clear evidence of 4f–5d hybridization was found [86]. Later, with the same theoretical methodology, the electronic structure and magnetic ordering of ErN and ErAs was investigated [87].

In 2005, Duan *et al* reported on the effect of strain on the electronic and magnetic properties of GdN [88]. The results of LSDA$+U$ indicate that GdN is nominally a ground-state half-metal at the experimental lattice constant, but it may undergo a phase transition to a semiconductor with lattice expansion. Soon thereafter, these studies were extended to the electronic structure and magnetic ordering of the GdX monopnictides [89]. Duan *et al* provided a quantitative analysis of the RKKY and superexchange interaction [90] of the GdX monopnictide systems.

As previously indicated, a number of rare-earth pnictides appear to resemble ground-state half-metallic ferromagnets. Johannes and Pickett studied the electronic structure and magnetic exchange interactions in EuN and EuP also using the FLAPW method [91]. They found that EuN is a ground-state half-metallic ferromagnet within conventional LSDA $+ U$ band theory. Ghosh *et al* studied the electronic, magnetic and optical properties of GdX in 2005 [92], with LMTO in the LSDA $+ U$ scheme. They also found that GdN is half-metallic if no further adjustment is implemented. Using LMTO within the LSDA $+ U$ approach, Larson and Lambrecht [93] found that by putting the Hubbard U on the d orbital as well, GdN is found to be a semiconductor; otherwise it is half-metallic, as noted by others [70, 88].

3.3. GW approximation (GWA)

Eigenvalues of the Kohn–Sham equations [94] are often interpreted as single-particle energies and are compared with photoemission spectra. This is not really justified and in many cases leads to incorrect predictions. A proper way to interpret the photoemission spectra is to use quasiparticle concepts [95]. The quasiparticle energies E_i can be obtained [96] from

$$\left[-\tfrac{1}{2}\nabla^2(\mathbf{r}) + V(\mathbf{r})\right]\Psi_i(\mathbf{r}) + \int \mathrm{d}^3r' \, \Sigma(\mathbf{r}, \mathbf{r}'; E_i)\Psi_i(\mathbf{r}') = E_i\Psi_i(\mathbf{r}), \qquad (6)$$

where the self-energy Σ addresses the effect of exchange and correlation and is intrinsically a non-local operator. The calculation of Σ is, however, generally very difficult and requires some approximations. In the so-called *GW* approximation (GWA) [97], Σ is obtained by the Green's function method:

$$\Sigma(\mathbf{r}, \mathbf{r}', E) = \frac{\mathrm{i}}{2\pi} \int \mathrm{d}\omega \, G(\mathbf{r}, \mathbf{r}'; E - \omega)W(\mathbf{r}, \mathbf{r}'; \omega); \qquad (7)$$

here G stands for the Green's function, and W is the screened Coulomb interaction, which can be evaluated by the random phase approximation (RPA) [98], i.e. assuming the electrons are non-interacting when they respond to the external and induced field.

The application of GWA to realistic materials was first carried out by Hybertsen and Louie in the 1980s [99]. Godby *et al* [100] obtained similar results using same approach. Due to the complexity in calculating the self energy, the application of the GWA to rare-earth compounds has not been undertaken until recently (for a recent review on GWA calculations, see [101]). Van Schilfgaarde *et al* [102] have drawn attention to their quasiparticle self-consistent *GW* (QSGW) calculations on Gd, GdP and GdAs. The QSGW calculations overestimate the position of the minority Gd f shell by ∼4 eV. The details of these calculations are not yet available.

In 2000, using the LMTO method and assuming that the quasiparticle energy gap corrections scale inversely with the dielectric constant, Lambrecht [103] predicted that GdN is a narrow indirect band gap insulator. He also claimed that, by applying a magnetic field, the band gaps can be tuned by aligning the Gd 4f magnetic moments.

3.4. Dynamical mean-field theory (DMFT)

Dynamical mean-field theory (DMFT) is a more modern, non-perturbative method that has proven to be successful in investigating strongly correlated systems with local Coulomb interactions [104]. This theory was initially developed from the *local impurity self-consistent approximation* [105], which is the natural generalization of quantum many-body problems of the Weiss mean-field theory [106]. DMFT is believed to be a major step towards the reunion of two theoretical approaches, i.e. the DFT and many-body model Hamiltonian of condensed matter physics.

The spirit of DMFT is to map a lattice problem with many degrees of freedom onto an effective single-site (impurity) problem with fewer degrees of freedom. DMFT becomes *exact* in the limit of high lattice coordination numbers [105]. The underlying physical idea is that the dynamics, at a given site, may be considered to be the interaction of the degrees of freedom at this site with an external bath created by all other degrees of freedom on other sites, a *dynamical* mean-field approximation [106]. This impurity problem has to be solved self-consistently together with the k-integrated Dyson equation connecting the frequency-dependent self-energy $\Sigma(\omega)$ and the on-site Green function G at frequency ω:

$$G(\omega) = \frac{1}{V_{\rm B}} \int {\rm d}^3k \frac{1}{\omega + \mu - H^0_{\rm LDA}(\mathbf{k}) - \Sigma(\omega)}, \tag{8}$$

where μ is the chemical potential, $H^0_{\rm LDA}$ is the one-particle Hamiltonian without the local Coulomb interaction, and $V_{\rm B}$ is the volume of the Brillouin zone.

Many techniques have been applied to solve the Anderson impurity model, such as quantum Monte Carlo, iterative perturbations, the fluctuation exchange approximation, the mean-field slave boson approach and the numerical renormalization group [104]. With these efforts, it is now possible to combine DMFT with modern electronic structure calculations to carry out LDA + DMFT [107] or spectral DFT [108] calculations.

The DMFT method has been successfully used to explain the $\alpha-\gamma$ transition in cerium, the δ-phase of plutonium and several Mott insulators [104]. In 1998, Lægsgaard and Svane [109] calculated the excitation spectra of the Ce monopnictides CeN, CeP, and CeAs using the DMFT method, with parameters obtained from *ab initio* atomic and LMTO band structure calculations. The theoretical spectra are in good agreement with experiment. Recently, Sakai *et al* [110] also carried out a DMFT calculation on CeSb.

3.5. Other theoretical approaches

There are also several calculations of rare-earth monopnictides using other approaches. Kalvoda *et al* studied the cohesive properties of GdN clusters using a quantum chemical (Hartree–Fock) method in 1998 [111]. They obtained a reasonable lattice constant for GdN (1.3–2.0% larger than the experiment values), but the details concerning the electronic structure were not presented.

Combining a many-body model (multi-band Kondo lattice model) and '*ab initio*' band structure calculations (LMTO), Santos *et al* studied the ferromagnetism and the temperature-dependent electronic structure of hexagonal close-packed (hcp) Gd in 2004 [112]. Later, using the same approach, Sharma and Nolting studied temperature-dependent electronic correlation effects in GdN in 2006 [113]. Assuming GdN to be a semiconductor, they obtained its quasiparticle spectral densities and density of states and found that the correlation effects were strongly temperature dependent. Using the s–f model, Bhattacharjee and Jaya, in 2006 [114], studied correlation and temperature effects on the electronic structure of bulk and thin film GdN. Bhattacharjee and Jaya also found a red shift of the GdN conduction bands with respect to temperature. Without any special treatment of the 4f states, Landrum calculated the electronic structure of CeN in 1999 using the LMTO method [115].

In summarizing the various theoretical approaches, discussed above, all have their advantages and drawbacks. For instance, because of the localized nature of the strongly correlated electrons, most of the theoretical methods, except for the GWA, were first developed using the LMTO method, which is based on a local orbital basis, as a starting point. For 4f systems, the SIC + LSDA method sometimes overestimates the separation between the occupied and unoccupied f states [70]. The LSDA + U method now has been implemented into several band structure schemes, due to its relatively simple physics, and thus is more widely accepted. The Hartree–Fock approximation treatment in the LSDA + U scheme to the on-site Coulomb interactions is, however, too crude for strongly correlated systems [107]. This approach is successful in describing the long-range ordered insulating states of correlated systems, while it fails to describe correctly the strongly correlated paramagnetic states. GWA and DMFT methods are believed to be more accurate than many other strategies in describing the strongly correlated systems. At this stage, the GWA and DMFT approaches are still too cumbersome to be used by the whole theory community.

Nevertheless, concepts like the Hubbard U and the self-energy Σ are now being widely adopted [73, 107]. In addition, the Wannier functions make it possible to set up localized orbitals through a plane wave basis [116, 117]. We expect that there will be many more *ab initio* studies on strongly correlated systems over the next few years.

3.6. Experimental studies

A series of ESR measurements has been carried out on single crystals of GdAs [118], GdP [119] and GdBi [120] since 2000. The magnetic structure of these compounds was confirmed to be antiferromagnetic (AFM) type II. The Fermi surface and magnetic properties of TbSb were investigated by Nakanishi *et al* in 2004 [121] using de Hass–van Alphen and high-field magnetization measurements.

In 2005 Leuenberger *et al* [122] reported electronic and magnetic properties of high-quality thin films of GdN. They found that a 500 Å thick GdN film exhibits physical and magnetic properties close to that of bulk GdN. The element specific x-ray magnetic circular dichroism (XMCD) measurements clearly demonstrated that the N p states are magnetically polarized. This agrees with theoretical predictions, as will be shown later. Leuenberger and
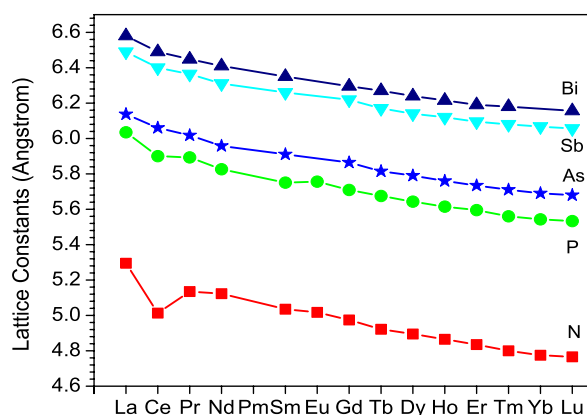
Figure 1. Lattice constants of rare-earth monopnictides: RN (squares), RP (circles), RAs (stars), RSb (down triangles), RBi (up triangles).

co-workers also found that the electrical conductivity of GdN is thermally activated down to the ferromagnetic T_c, below which GdN exhibits metallic character. They attribute the origin of this semiconductor–metal transition to a non-stoichiometric GdN film, similar to that found for EuO [123, 124]. Later experiments demonstrated a significant reduction of T_c as a result of the influence of lattice expansion [125], as predicted by theory [88]. More recently, Granville *et al* [126] claimed that GdN is semiconducting in both paramagnetic and ferromagnetic states ($T_c = 68$ K). The suggestion was that the N vacancies may be responsible for the conductivity in GdN.

As a final note, although tangential to GdN, Leuenberger and co-workers [127] also found that Fe layers induce long-range magnetic order in GdN layer at temperatures above the T_c of GdN in GdN/Fe multilayers.

4. Electronic, magnetic and transport properties

There are many similarities among the rare-earth monopnictide family, and some stunning differences with regard to metallicity and magnetic ordering. This is summarized in table 1, which lists the experimental lattice constants of all the rare-earth monopnictides, together with their magnetic ordering, transition temperatures and metallicity, i.e. insulating (semiconducting) or (semi)metallic, for most of the more than 60 compounds in the rare-earth monopnictide family. Most of the rare-earth monopnictide family have the NaCl-type structure (space group $Fm\bar{3}m$). EuAs, EuSb and EuBi do not adopt the NaCl-type structure, and have been omitted in table 1. There are no experimental reports for the Pm monopnictides, most probably due to the fact that Pm must be artificially prepared. We are also unable to find any report on YbBi.

From table 1, we can see that the lattice constants of rare-earth monopnictides, as a general trend, increase from N to Bi but decrease from La to Lu: the lattice constant typically decreases with increasing 4f occupancy, as indicated in figure 1. This trend in the lattice constant can be simply explained by the increase of anion sizes and the decrease of cation sizes with the increase of atomic number. Not surprisingly, the smallest lattice constant belongs to LuN (4.766 Å), and the largest to LaBi (6.580 Å): a difference of about 38%. We note that there are exceptions to this general trend: for example, CeN, SmP. As shown in the experiments of Olcese [128] and theoretical calculations by Aerts *et al* [70], the jump in lattice constants from CeN to PrN is due to the fact that the ground state for Ce in CeN is tetravalent instead of trivalent.

Table 1. Physical and magnetic properties of rare-earth monopnictides. Unless explicitly indicated, the data are collected from [39]. 'Metallicity' values are band gaps in eV derived from optical absorption of thin films if the material is an insulator or semiconductor. SC means semiconductor, SM means semimetal.

		N	P	As	Sb	Bi
La	a (Å)	5.295[a]	6.035[b]	6.137[c]	6.490[d]	6.577[e]
	Metallicity	SC, 0.82			SC, 0.7–0.8	
Ce	a (Å)	5.013[a]	5.90	6.06	6.40	6.49
	Ordering	No order	AFM-I	AFM-I	AFM	AFM
		down to 1.5 K			(complicated)	(complicated)
	$T_{N(C)}$ (K)		6–7, 8.5, 9	5–7.5, 7.5	16, 18	25, 25.5, 26
	Metallicity	SM[f]	SC, 1.1	SC, 0.7	SM[f]	
Pr	a (Å)	5.135[g]	5.893	6.018	6.364	6.448
	Ordering					
	$T_{N(C)}$ (K)					
	Metallicity	SC, 1.03		SC, 1.0	SC, 0.66	
Nd	a (Å)	5.123[a]	5.826	5.958	6.31	6.41
	Ordering	FM	AFM-I	AFM-I	AFM-I	AFM-I
	$T_{N(C)}$ (K)	27.6, 29, 32, 35	7, 11	10.6, 12.5, 13	15.5, 16	24, 25
	Metallicity	SC, 0.8		SC, 1.04		
Sm	a (Å)	5.035	5.75	5.91	6.26	6.35
	Ordering	AFM	AFM	AFM	AFM	AFM
	$T_{N(C)}$ (K)	<2, 13, 18	1.65	1.8	2.1, 2.8	8.6
	Metallicity	SC, 0.7	SC, 1.09	SC, 1.03	SC, 0.59	
Eu	a (Å)	5.017[h]	5.756[i]	—	—	—
	Ordering					
	$T_{N(C)}$ (K)					
	Metallicity	SC, 0.76				
Gd	a (Å)	4.974[j]	5.709[j]	5.864[j]	6.219[j]	6.295[j]
	Ordering	FM[j]	AFM-II[j]	AFM-II[j]	AFM-II[j]	AFM-II[j]
	$T_{N(C)}$ (K)	58.0[j]	15.9[j]	18.7[j]	23.4[j]	25.8[j]
	Metallicity	SC, 0.98, 0.85	SM[j]	SM[j]	SM[j]	SM[j]
Tb	a (Å)	4.922	5.675	5.815	6.17	6.27
	Ordering	FM, AFM[k]	AFM-II	AFM-II	AFM-II	AFM-II
	$T_{N(C)}$ (K)	T_C: 34, 39, 42 T_N: 31[k]	8, 9	10.5, 12	14, 15, 16.5	17, 18
	Metallicity	SC, 0.8		SC, 0.7	SC, 0.35	
Dy	a (Å)	4.895	5.643	5.79	6.14	6.24
	Ordering	FM, AFM	Flop-side FM	Flop-side FM	AFM-II	AFM-II
	$T_{N(C)}$ (K)	T_C: 17, 17.6, 26 T_N: 15	4.5, 8	8.5	9.5, 12	12, 13
	Metallicity	SC, 0.91, 0.95	SC, 25	SC, 0.9, 1.0		
Ho	a (Å)	4.865	5.615	5.76	6.12	6.215
	Ordering	FM	Flop-side FM	AFM-II	AFM-II	AFM
	$T_{N(C)}$ (K)	11, 13.3, 18	5.5	4.8	5, 9	6.7
	Metallicity	SC, 0.73, 1.05	SC, 1.1–1.2	SC, 0.8	SC, 0.45	
Er	a (Å)	4.835[a]	5.595	5.734	6.095	6.19
	Ordering	FM	AFM-II	AFM-II	AFM-II	AFM
	$T_{N(C)}$ (K)	3.4, 4.5, 5, 6	2.3, 3.1	2.9, 3.5	3.55, 3.7	3.5, 3.9
	Metallicity	SC, 1.2, 1.3	SM[l]			
Tm	a (Å)	4.80	5.56	5.71	6.08	6.18
	Ordering	No order down to 1.3 K				
	$T_{N(C)}$ (K)					
	Metallicity	SC, 1.1		SC, 1.18		

Table 1. (Continued.)

		N	P	As	Sb	Bi
Yb	a (Å)	4.775	5.543	5.69	6.067	—
	Ordering	AFM	AFM	AFM		
	$T_{N(C)}$ (K)	0.75[m]	0.66[m]	0.55[m]		
	Metallicity	SM[n]	SM[n]	SM[n]		
Lu	a (Å)	4.766[o]	5.533[p]	5.68[p]	6.056[p]	6.156[p]
	Metallicity	SC, 1.55, 1.6				

[a] Reference [128]. [b] Reference [130]. [c] Reference [131]. [d] Reference [132]. [e] Reference [133]. [f] Reference [134].
[g] Reference [135]. [h] Reference [136]. [i] Reference [137]. [j] Reference [60]. [k] Reference [138]. [l] Reference [51].
[m] Reference [139]. [n] Reference [53]. [o] Reference [140]. [p] Reference [141].

The bonding between the rare-earth atoms and pnictogen atoms cannot be simply described as ionic or covalent, otherwise all the rare-earth monopnictide family should be insulators (semiconductors). However, from N to Bi, we can see a gradual increase in metallicity in these compounds. The typical carrier concentrations in these compounds are around 10^{19}–10^{21} cm^{-3} [103], making them semimetals or highly doped n-type semiconductors.

In listing the known energy gaps for those rare-earth monopnictide compounds that are regarded as semiconductors, we note that the light pnictides, like the nitrides, tend to be larger energy gap semiconductors than the heavy pnictogen compounds. The changes in the energy gaps from La to Lu are rather scattered and it is hard to find a clear trend. We should point out that those data for energy gaps are not that reliable, since the electronic and transport properties are strongly affected by impurity dopants; thus a number of controversies exist in the comparison of various experiments. For example, GdP, GdAs and GdSb were thought to be semiconductors [39], but later experiments on high-quality samples clearly showed that they are actually semimetals [47, 57].

The magnetic ordering of rare-earth monopnictides is also quite complicated, ranging from ferromagnetic (FM), flip-flop FM [22], to to be AFM type II. Three typical AFM configurations (also see [129]) are depicted in figure 2. As we can see from table 1, most monopnictides have AFM ground states with exceptions among the nitrides and phosphides. Overall, we can see that the magnetic interactions gradually increase from La to Gd (FM, 58 K), then decrease again from Gd to Lu. With the increase of anion sizes, the FM pnictides become AFM and the Néel temperature increases. Apparently, HoP and DyP are in the intermediate region between FM and AFM, as flip-flop FM can be regarded as combination of a FM and an AFM configuration [22]. This balance between AFM and FM ordering may also be the reason that CeN and TmN have no apparent net magnetic order.

The electronic structure calculations on three typical rare-earth pnictides, based on the LSDA + U scheme with FLAPW method [86], confirm some of these trends and also can illustrate the effect of changing the lattice constant, without changing the pnictide, which is not easily done in experiment. For convenience, the Brillouin zone of the face-centred cubic (fcc) lattice is shown in figure 3, together with definitions of some high-symmetry k-points and k-lines.

4.1. Gd monopnictides

Among all the rare-earth monopnictides, the Gd monopnictides have been and continue to be studied extensively, nonetheless, there still remains intense controversy regarding their electronic structure and transport properties [31, 36, 43, 58, 70, 88, 93, 103, 122, 126]. This
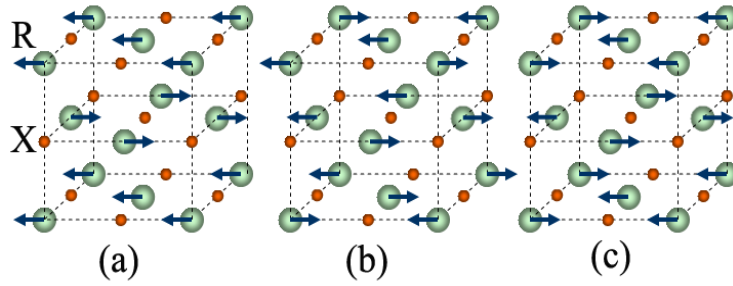
Figure 2. Three antiferromagnetic ordering configurations in rare-earth monopnictides: (a) AFM-I, (b) AFM-II, (c) AFM-III. Arrows indicate magnetic moment orientations on rare-earth atoms.
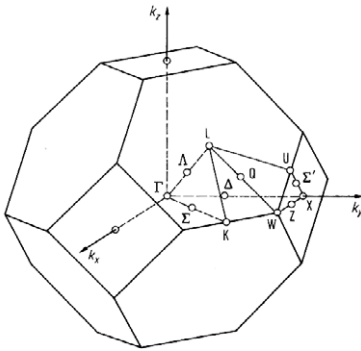

Figure 3. The Brillouin zone of the face-centred cubic lattice.

is especially true for GdN. Various calculations have been undertaken on different magnetic phases (FM and AFM) with different schemes (LSDA and LSDA + U) of GdX (X = N, P, As, Sb, Bi). The electronic structures, typical for rare-earth monopnictides, are presented in the discussion that follows.

Figure 4 shows the band structure of GdN in the FM state with and without on-site 4f Coulomb interactions. To construct the band structure in figure 4, we used an effective Hubbard $U_{\text{eff}}^{4f} = U - J = 9.2$ eV for Gd compounds in the LSDA + U scheme. As we will show later, this value gives much better agreement with experiment on the 4f energy levels than previous values did in the study of Gd metal or Gd compounds [142–144, 88, 89], i.e. $U = 6.7$ and $J = 0.7$ eV.

As can be seen from figure 4(a), the LSDA + U strategy has no significant impact on the whole LSDA band structure of GdN, except upon the energy levels of the occupied and unoccupied 4f states. In the pure LSDA scheme, the occupied 4f states are placed about 3.2 eV below E_F, strongly hybridized with N 2p states, while the unoccupied 4f states are located about 2 eV above E_F, mixed with Gd 5d states. There is no direct photoemission data from GdN single crystals, but experiments on GdP (As, Sb, Bi) show that the occupied and unoccupied 4f levels are situated 8–10 and 5–6 eV below and above E_F, respectively [59]. Furthermore, the x-ray photoelectron spectroscopy (XPS) experiments on GdN films show that the Gd 4f levels are 7.8 eV below E_F [122]. Thus the LSDA calculation fails to give the correct 4f energy level binding energies. This situation is much improved by the LSDA + U method (figure 4(b)). In fact, now the unoccupied 4f states remain around 6.6 eV above E_F, and the occupied 4f states are 7.8 eV below E_F, in very good agreement with experiments.
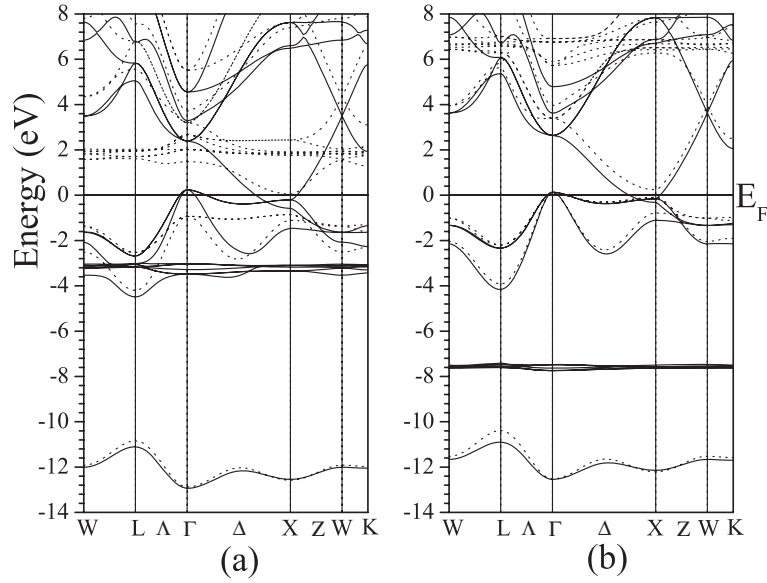
Figure 4. Electronic structure of ferromagnetic GdN for experimental lattice constants (a = 4.974 Å): (a) LSDA, (b) LSDA + U with U_{eff} = 9.2 eV. Solid and dotted lines represent spin majority and spin minority states, respectively.

Figure 4(b) is actually qualitatively representative and contains most of the typical features of the band structure of most rare-earth monopnictides. The pnictogen p-derived states (here N 2p) dominate the top of the valence bands. Precisely speaking, these pnictogen p states are actually hybridized with rare-earth (here Gd) 5d (6s) states, which dominate the bottom of conduction band. This hybridization results in a hole pocket at the Γ point and an electron pocket at the X point in metallic pnictides. The numbers of electrons and holes are the same [31]. Even if the rare-earth pnictides are determined to be semiconductors, the close proximity (and likely Fermi level crossing) of the unoccupied rare-earth 5d states near the X point would make the energy gap indirect. A significant exchange splitting can be found in the band structure, and this is indeed the origin of the nominal half-metallicity in rare-earth monopnictides, as we will discuss in detail later.

The *l*-projected density of states (DOS) plot (figure 5) provides an even clearer picture of the elemental contributions to the electronic structure of GdN. As one can see, those top valence states right below the Fermi level are predominantly N 2p states. The Gd d states, however, also make a noticeable contribution. Note here that in our calculation both 5d e_g and 5d t_{2g} states participate in the hybridization with N 2p states, though the contributions to the bottom of the conduction band(s) are dominated by 5d t_{2g} states. Not only do the calculated 4f levels agree well with experiment, but the Gd 5p states are located at the same binding energy position (about 21 eV below E_F) found in experiment [122]. The 1.8 eV separation between the Gd 5p majority and minority states is caused by the exchange splitting. We would like to point out that the Gd 5d–X 2p hybridization is important in establishing the physical properties of GdX. This hybridization results in magnetic moments on pnictogen sites and is responsible for the intriguing magnetic orderings and transport properties.
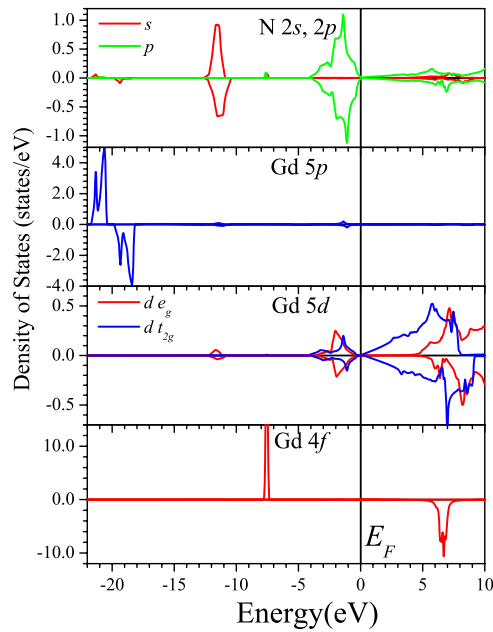
Figure 5. The *l*-projected DOS of GdN. Spin minority states are of negative values.

Band structures for other Gd monopnictides in the ferromagnetic state, using $LSDA + U$, are shown in figure 6. Note that the magnetic ground states of these compounds are AFM-II type. We can consider these structures as the saturated limit of the paramagnetic states in a magnetic field [36].

The band structures seen for the rare-earth pnictides from GdN to GdBi are quite similar, except that for GdSb and GdBi there are no gaps between the Gd 5d states and pnictogen p states at the Γ point. We find that, with a single universal $U_{\mathrm{eff}}^{4\mathrm{f}}$, the f levels in these compounds, both occupied and unoccupied, are all in excellent agreement with experimental observations [59, 122], vindicating the application of the $LSDA + U$ scheme. This is clearly shown in the XPS and x-ray bremsstrahlung isochromat spectroscopy (X-BIS) spectra of GdX (figure 7). There exists a monotonic energy down shift from GdN to GdBi [59], which is clearly represented in the $LSDA + U$ band structures of GdX.

From the $LSDA + U$ calculations, all the Gd monopnictides are seen to be semi-metallic except for GdN, which is nominally half-metallic with a half-metallic gap about 0.5–0.6 eV. Experimentally, the GdP (As, Sb, Bi) pnictides are found to be metallic [58]. For GdN, as noted previously, the experimental temperature-dependent resistivity of the GdN film [126] shows a picture (figure 8) that differs from other GdX compounds (figure 9, [58]). The high-temperature behaviour of the resistivity of GdN is more like that of a semiconductor, apparently different from other Gd monopnictides. The resistivity peak around the transition temperature can be explained by the long-range magnetic ordering which significantly decreases the spin-dependent scattering of charge carriers, well below the transition temperature. The broad range of this peak may be attributed to the imperfection periodicity or the Kondo-lattice model [145, 146]. Though the resistivity at very low temperature is not huge (5 Ω cm), it is again still more like a semiconductor.

If GdN is really a semiconductor, with an optical gap about 1.5–2 eV [126], then it means that there still is something important missing in the '*ab initio*' calculations. Lambrecht [103],
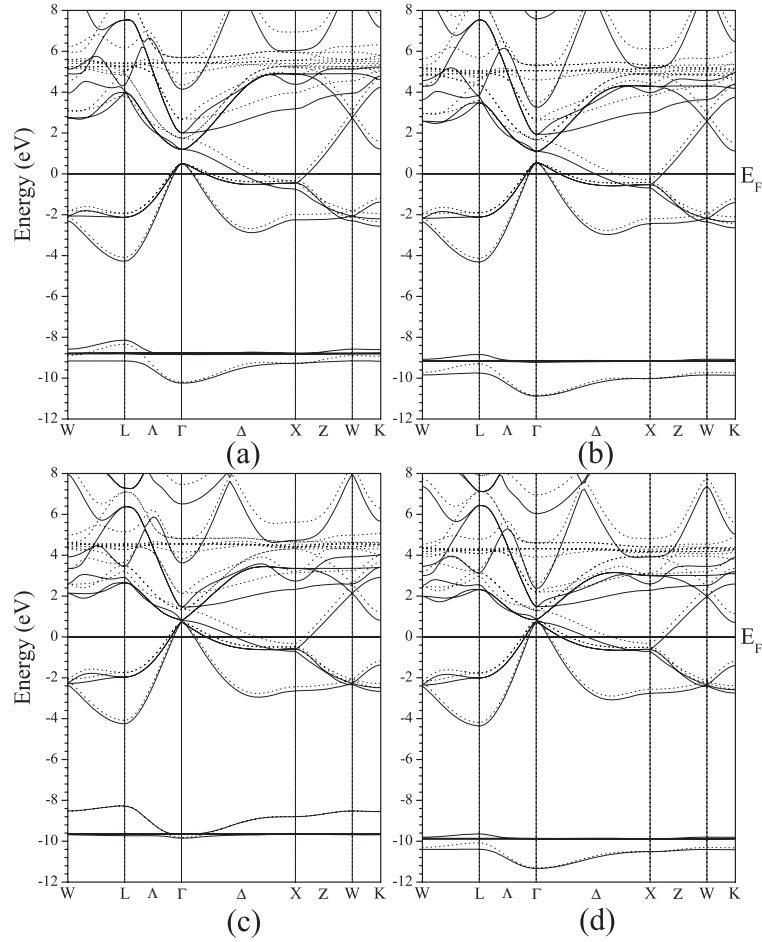
Figure 6. Electronic structure (LSDA $+ U$ with $U_{eff} = 9.2$ eV) of (a) GdP ($a_{exp} = 5.709$ Å), (b) GdAs ($a_{exp} = 5.864$ Å), (c) GdSb ($a_{exp} = 6.219$ Å), (d) GdBi ($a_{exp} = 6.295$ Å) in the ferromagnetic phase.

Ghosh *et al* [92], Larson and Lambrecht [93] used different approaches to shift the Gd 5d bands and managed to make GdN semiconducting. These empirical treatments of the theory do not give the correct positions of the Gd 4f levels. Apparently, more effort is needed to fill the persistent gap between theory and experiment.

Since the ground states of GdX (X = P, As, Sb, Bi) are all of AFM-II type (see figure 2(b)), it is interesting to compare the difference between the AFM and FM electronic structures. Figure 10 shows both AFM and FM bands of GdP with the same rhombohedral cell (where the Brillouin zone is shown in figure 11) and adopting the experimental lattice constants. As we can see, the AFM bands show an average effect of the FM spin majority and minority bands, and this leads to a small reduction in total energy. The essential feature of the electronic structure, however, remains the same.

From the above analysis, apparently GdN is on the border between semiconductor and semimetal states. Thus the GdN physical properties are very sensitive to non-stoichiometry, impurities, pressure, temperature, magnetic field, etc. In addition, exotic phenomena, such as
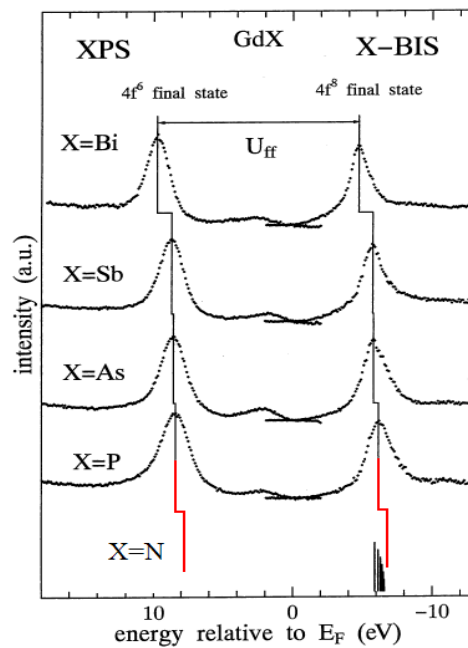
Figure 7. The XPS and X-BIS spectra of GdX (X = P, As, Sb, Bi) (from [59]). Vertical line indicating the occupied 4f level of GdN is from [122], the unoccupied GdN 4f level is calculated using the U_{ff} indicated in the figure.
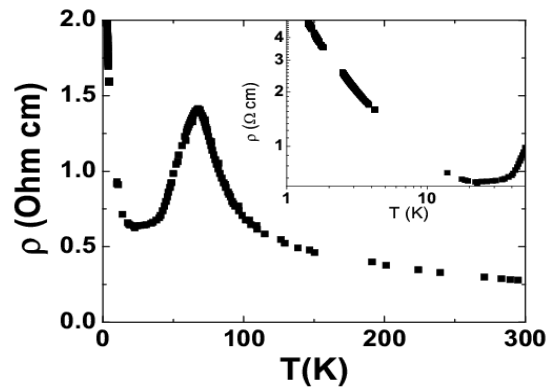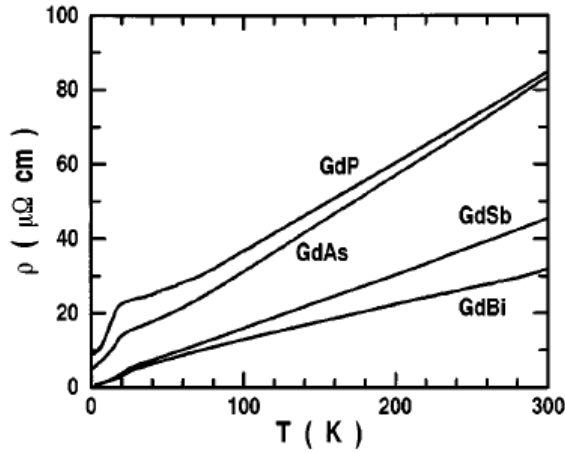

Figure 8. Temperature-dependent resistivity of a 200 nm thick GdN film. The pronounced peak at 68 K corresponds to the measured Curie temperature of the film. The inset shows the low-temperature behaviour of the resistivity (from [126]).

electron–hole liquids [147], may occur in the region between semiconductor and semimetal states. Again, if it is true that GdN is a semiconductor and GdP is a semimetal, then most probably there should exist some GdN–GdP alloys that would be nominally half-metallic.

4.2. Eu monopnictides

In the europium pnictide family only EuN and EuP crystallize with fcc structure. According to Hund's rules [148], the ground state of Eu^{3+} ($4f^6$) is $^7F_0$, i.e. $S = 3$, $L = 3$, $J = 0$. Thus

Figure 9. Temperature-dependent resistivity of stoichiometric GdX (X = P, As, Sb, Bi) single crystals measured at zero field (from [58]).
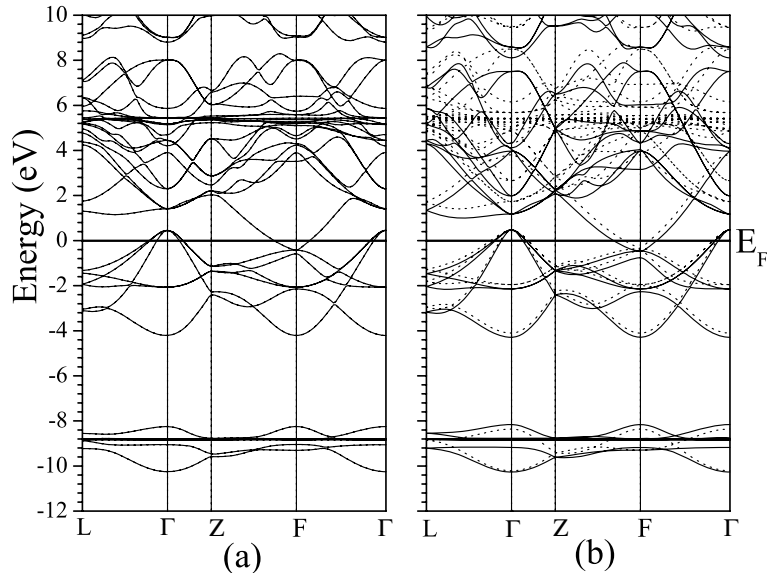

Figure 10. Electronic structure of GdP with rhombohedral cell: (a) antiferromagnetic phase (AFM-II), (b) ferromagnetic phase. Note that in antiferromagnetic phase there is no difference between the spin majority and minority states.

isolated Eu^{3+} is supposed to be non-magnetic. In the crystalline environment, however, the orbital moment generally will be suppressed by the crystal field; thus net magnetic moments may exist in EuX (X = N, P). In addition, as in the case of Gd monopnictides, there could be induced magnetic moments on pnictogen atoms. Taking into account the spin–orbit coupling, bulk Eu^{3+} could exhibit significantly different magnetic properties from that of isolated Eu^{3+}.

Experimental studies on the electronic structure of the EuX (X = N, P) compounds are very rare. Theoretical calculations are also limited. So far there have only been two published calculations on europium monopnictides, to our knowledge. As previously noted, Horne *et al* reported EuN to be half-metallic based on the SIC–LSDA method [71] and was confirmed by Johannes and Pickett [91] using the LSDA + U scheme.
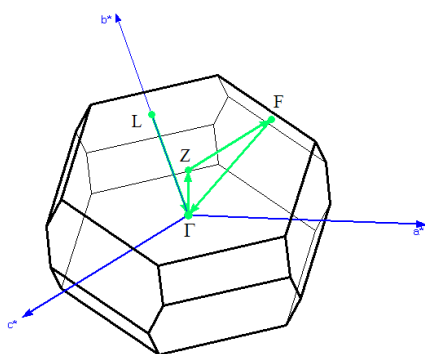
Figure 11. The Brillouin zone of the rhombohedral lattice.
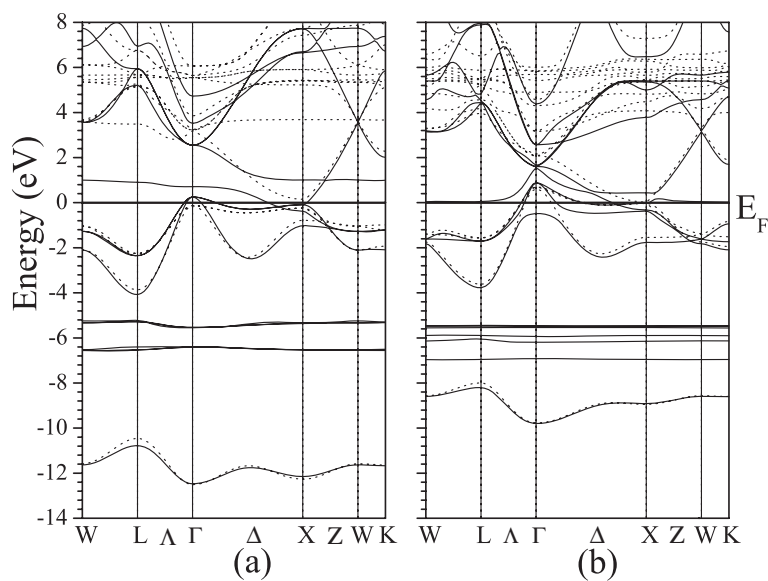
Figure 12. Electronic structure (LSDA + U with $U_{\text{eff}} = 7$ eV) of (a) EuN ($a_{\text{exp}} = 5.017$ Å) and (b) EuP ($a_{\text{exp}} = 5.756$ Å) in ferromagnetic phases.

Following Johannes and Pickett [91], using the LSDA + U approach with U and J set as 8 and 1 eV respectively, we have obtained similar band structures for EuN and EuP, as shown in figure 12. The spin–orbital effects were not considered in these calculations and will be discussed later. Johannes and Pickett's calculations showed that the ground states of EuN and EuP are FM and AFM-II, respectively. Here we only present results of the FM states of two compounds for comparison. The difference between the FM and AFM states of EuP is very similar to the case of GdP (figure 10).

As we can see from figure 12, the band structures of Eu monopnictides are similar to those of Gd monopnictides (figures 4 and 6). The major differences arise from the unoccupied 4f majority states. In EuN, this state is about 1 eV above E_{F}, whereas in EuP this state crosses the Fermi level. In both cases, the unoccupied 4f states are strongly hybridized with Eu 5d and pnictogen p states. Figure 12(a) shows that, in this conventional LSDA + U band calculation, EuN is half-metallic with a 0.5 eV gap in the minority spin channel. Other Eu monopnictides are semimetallic, like EuP, as illustrated in figure 12(b).
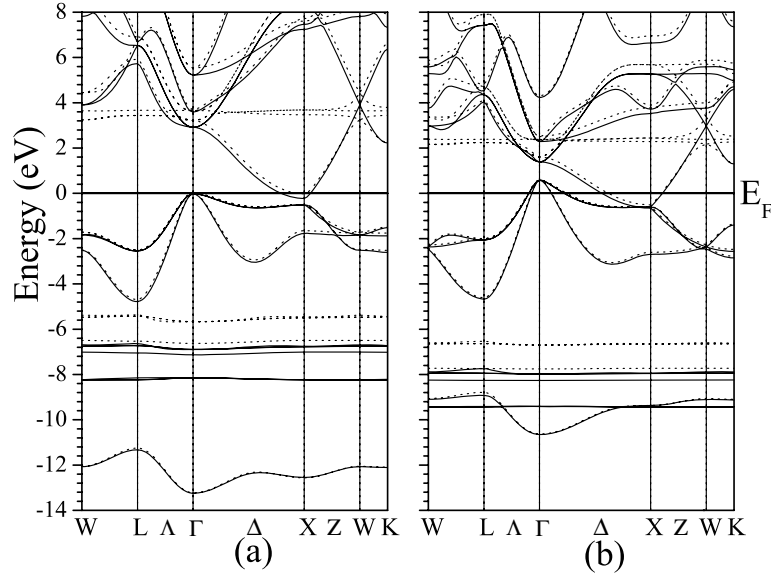
Figure 13. Electronic structure (LSDA + U with $U_{\mathrm{eff}} = 7.85$ eV) of (a) ErN ($a_{\mathrm{exp}} = 4.835$ Å), (b) ErP ($a_{\mathrm{exp}} = 5.595$ Å) in ferromagnetic phases.

4.3. Er monopnictides

Er^{3+} represents another type of rare-earth ion, which has more than a half-filled 4f electron shell. This provides a contrast with Gd (with a half-filled 4f electron shell) and Eu (with a less than half-filled 4f electron shell). The ground state of isolated Er^{3+} ($4f^{11}$) is $^4I_{15/2}$, i.e. $S = 3/2, L = 6, J = 15/2$. Only ErAs has been studied extensively experimentally [50, 51, 84], whereas theoretical studies of all of the Er monopnictides have been undertaken [35, 36, 70, 84, 85, 87]. Except for ErN, all Er monopnictides have AFM ground states and have similar electronic structures and physical properties, nonetheless, here we present our LSDA + U band calculations for ErN and ErP in the ferromagnetic state (figure 13). Following Komesu *et al* [84], U and J are chosen to be 8.6 and 0.75 eV, respectively.

In the Er monopnictides, all the 4f majority states and four of the seven 4f minority are occupied. Because of the Coulomb repulsion, the unoccupied 4f states reside 3.2–3.6 eV above E_F in ErN. A zero half-metallic gap is found for ErN in the LSDA + U band calculations, whereas ErP is semimetallic in both spin channels with the 4f bands shifted down about 1 eV (figure 13).

5. Half-metallicity and other interesting phenomena

5.1. Origins of half-metallicity

In band calculations, half-metallicity will not occur if there is no exchange splitting. While an exchange splitting is a necessary condition for half-metallicity, exchange splitting alone is not sufficient, even in the rare-earth monopnictides. The exchange splitting must be large enough to form a gap between the unoccupied and occupied states in one spin channel and at the same time the other spin channel should be partially occupied. Thus the formation of half-metallicity strongly depends on the magnitude of exchange splitting as well as the details of the electronic structure. For a perfect ionic or covalent crystal, the exchange splitting is zero due
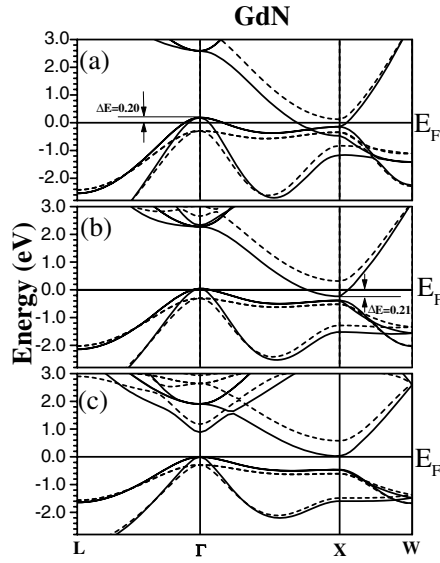
Figure 14. The LSDA + U (U_{eff} = 6.0 eV) band structure of GdN in the vicinity of the Fermi energy for three volumes: (a) at the calculated equilibrium lattice parameter a = 4.92 Å, (b) at the lattice parameter increased by 5% (a = 5.16 Å), (c) at the lattice parameter increased by 14% (a = 5.63 Å). Solid and dotted lines represent spin majority and spin minority states, respectively. The change of conducting properties is indicated by the change of energy difference between the top (bottom) of the hole (electron) pockets and the Fermi energy (from [88]).

to the fully occupied outermost electron shell, which also makes the system insulating. For a partially occupied electron shell, the exchange splitting is generally around 0.1–1.5 eV in most elements and compounds, whereas the width of unoccupied bands is generally above 3–4 eV. As a consequence half-metallic materials are rather rare.

In some sense, the band structure of rare-earth monopnictides resembles another class of nominally half-metallic materials: the full-Heusler alloys [149]. In the band structure there is a hole pocket around the Γ point and a electron pocket around the X point (figure 4). The spin exchange splitting is of opposite sign for the top valence and bottom conduction bands, i.e. the exchange splitting pushes the majority states to the top of the valence band (at the Γ point) and simultaneously pushes down the minority states (at the X point). Thus, under some conditions, a gap forms in the spin-down channel in some calculated band structures.

Rare-earth systems are known to exhibit band- and wavevector-dependent exchange splitting [9, 11, 150, 151]. Taking GdN as an example, we see that the Gd 5d states are polarized by the 4f majority states, due to exchange interactions and 4f–5d orthogonality. This means that the Gd 5d majority spin states, which dominate the bottom conduction bands, are shifted to greater binding energies. At the same time, the Gd 5d states are hybridized with N 2p states. This hybridization shifts up the N 2p majority spin states, resulting in the exchange splitting at the top valence bands, which mainly consist of the N 2p electrons. This shift in weight from Gd 5d to N 2p does result in a wavevector-dependent exchange splitting. We note that the exchange splitting is also Hubbard U dependent, as can be seen from the differences between figures 4(b) and 14(a). This is because the larger U of the f states means fewer f–d interactions, and thus a smaller exchange splitting.

Another by-product of the above Gd 5d–N 2p hybridization is the induced magnetic moments on nitrogen atoms. Actually, the induced magnetic moment on the pnictogen atom

is a typical feature of rare-earth monopnictides. This was first pointed out by Petukhov *et al* [36] and has been confirmed by recent experiments [122]. This induced pnictogen magnetic moment is antiparallel to that of the rare-earth atoms, with a magnitude in the range of 0.05–0.14 μ_B. Such an induced antiparallel magnetic moment on the non-magnetic atom is also found in magnetic interface structures, for example $Co/SrTiO_3$ [152, 153] and Fe/BTO [154], in which the non-magnetic Ti atom has a negative magnetic moment due to the Ti 3d–Fe 3d hybridization.

5.2. Metal–insulator transitions

We can see from table 1, figure 4 and figure 6 that the metallicity of rare-earth monopnictides gradually increases from N to Bi. Since experimentally most rare-earth nitrides are semiconductors, we can reasonably expect a metal–insulator transition in some rare-earth pnictide compounds or their alloys, due to impurity doping, temperature, pressure or even magnetic field.

Duan *et al* [88] studied both the volume and lattice strain effect on the electronic properties of GdN using $U_{eff}^{4f} = 6$ eV. The results are shown in figure 14. It is evident that, at larger volumes, the electron (hole) pockets become substantially shallower, meaning that the bottom (top) of the band approaches the Fermi energy and the area of the Fermi surface decreases. Both carrier density and carrier mobility decreases with an increase of the cell volume. Though it is hard to realize such a dramatic volume change in practice, the trend should be correct in the regimes that prove to be experimentally accessible. This transition is close to resembling a Mott metal–insulator transition, and such models [155] may be used to explain the gap in GdN found experimentally.

We note that there is another mechanism of metal–semiconductor transition, i.e. through d–f or s–f hybridization. In the famous Falicov–Kimball model [156], the single-electron states consist of extended Bloch functions and localized states centred on the metallic ions in the crystal. At low temperatures, the quasiparticle excitations are either localized holes or itinerant electrons. The electron–hole interaction may be responsible for the semiconductor–metal phase transition. The same spirit is presented in the electron–hole liquid theory [147], which is used to explain the ground state of ScN. Using a novel many-body theory and Kondo lattice model (s–f model), Kreissl and Nolting predicted that the decreasing magnetic order induces a transition from half-metallic to semiconducting behaviour in EuB_6 [157]. If this can be confirmed experimentally, then similar examples should be found among the rare-earth monopnictides.

5.3. Magnetic ordering

The magnetic properties are closely related to the electronic and transport properties in rare-earth monopnictides. For instance, a dramatic change of electric resistance has been found near T_c in GdN [122, 126]. Despite their rather simple fcc structure, the magnetic orderings of the rare-earth pnictides are very complicated [22, 23, 39, 54]. Based on the experience with rare-earth metals [9, 144], it is generally believed that there exists an indirect RKKY exchange interaction in the rare-earth pnictides. In 1997, Li *et al* estimated the exchange parameters of GdX from experimental data [60]. They attributed the sign change of exchange parameters to RKKY oscillations. Several groups believe that the superexchange interaction should also exist, and may dominate these compounds [88, 89, 91].

Duan *et al* [88, 89] proposed a systematic way to study the magnetic ordering in the rare-earth pnictide fcc structures. The basic strategy is to first deduce the exchange interaction
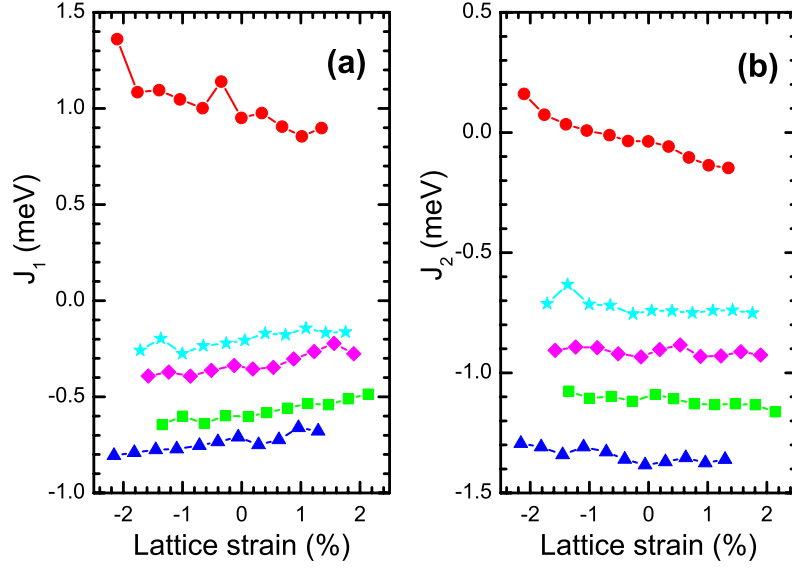
Figure 15. Calculated exchange parameters J_1 (a) and J_2 (b) for Gd pnictides as a function of the lattice strain: GdN (circles), GdP (stars), GdAs (diamonds), GdSb (squares), GdBi (triangles). The lattice strain is defined by the relative deviation of the lattice constant from the theoretical equilibrium lattice constant (from [89]).

parameters of GdX compounds by fitting the first-principles total energies of different magnetic configurations to those computed within the Heisenberg model,

$$H = - \sum_{n=1,2,3} J_n \sum_{i>j}^{n\text{th NN}} \mathbf{S}_i \cdot \mathbf{S}_j. \tag{9}$$

Here $\mathbf{S}_i$ is the unit vector in the direction of the magnetic moment at the ith lattice site, J_n is the exchange parameter between the nth nearest-neighbour (NN) magnetic atoms, and we limit our consideration to third-NN interactions. In this case the differences between the energy of the three AFM states E_n ($n =$ I, II, III) shown in figure 1 and the energy of the FM state E_{FM} are

$$
\begin{aligned}
\Delta E_{\text{I}} &\equiv E_{\text{I}} - E_{\text{FM}} = 8J_1 + 16J_3, \\
\Delta E_{\text{II}} &\equiv E_{\text{II}} - E_{\text{FM}} = 6J_1 + 6J_2 + 12J_3, \\
\Delta E_{\text{III}} &\equiv E_{\text{III}} - E_{\text{FM}} = 8J_1 + 2J_2 + 8J_3.
\end{aligned} \tag{10}
$$

The so-derived exchange parameters are then put into Monte Carlo simulations to calculate the transition temperatures of the compound. Results for GdX are shown in table 2.

The lattice constant dependences of the exchange parameters J_1 and J_2 are also obtained (figure 15). From the analysis of these data, Duan *et al* [89] proposed an expression for the superexchange interaction:

$$J_2^{\text{super}} = -n_d \frac{t_{\text{pd}}^4}{\Delta^3}, \tag{11}$$

where Δ is the energy difference between the rare-earth 5d orbital and the outmost p state of the pnictogen ion, n_d is the induced d moment on the rare-earth atom due to atomic 4f–5d exchange interactions, and the hopping parameter t_{pd} can be evaluated according to

Table 2. Calculated total energy differences per formula between ferromagnetic and three antiferromagnetic configurations for Gd monopnictides $\Delta E_n = E_n - E_{\text{FM}}$ ($n =$ I, II, III). Values inside the parentheses are calculated using the theoretical lattice constants. Theoretical and experimental transition temperatures [14] are listed for comparison (from [89]).

	a (Å) Exp.(Theor.)	ΔE_{I} (meV)	ΔE_{II} (meV)	ΔE_{III} (meV)	J_1 (meV)	J_2 (meV)	J_3 (meV)	$T_{\text{N(C)}}$ (K) MC	Exp.
GdN	4.97(4.92)	6.7(7.1)	4.2(5.1)	6.5(7.3)	0.86(0.95)	−0.14(−0.04)	−0.01(−0.03)	34(38)	58.0
GdP	5.71(5.63)	−2.8(−3.3)	−6.5(−6.9)	−3.5(−4.0)	−0.17(−0.21)	−0.74(−0.74)	−0.09(−0.11)	12(13)	15.9
GdAs	5.86(5.77)	−3.9(−4.3)	−8.4(−8.8)	−4.7(−5.4)	−0.22(−0.34)	−0.91(−0.93)	−0.13(−0.10)	14(16)	18.7
GdSb	6.22(6.11)	−5.7(−6.6)	−11.1(−11.5)	−7.2(−7.9)	−0.51(−0.60)	−1.13(−1.10)	−0.10(−0.11)	20(19)	23.4
GdBi	6.30(6.24)	−6.9(−7.3)	−13.4(−13.8)	−8.8(−9.3)	−0.66(−0.71)	−1.37(−1.38)	−0.10(−0.10)	22(23)	25.8

Harrison [158]. We should note here that the evaluation of equation (11) is quite empirical, since accurate determinations of Δ and other parameters are not available. Nevertheless, the estimated superexchange interactions in GdX are found to be AFM and have the same magnitude as the total effective magnetic interactions. These AFM superexchange interactions are strengthened when the size of the pnictogen atoms increases, and they eventually dominate the magnetic interactions in rare-earth pnictides. This picture agrees well with experimental observations [60]. Using similar technique, Larson and Lambrecht [93] also obtained the exchange parameters of GdX in good agreement with experiment.

Duan *et al* also investigated the magnetic dipole interactions and magnetic anisotropy effects in rare-earth monopnictides. They found that dipole–dipole interactions could play an important role in determining the magnetic behaviour of the rare-earth compounds, and are especially instrumental in the magnetic anisotropy, but they cannot solely account for stabilizing the magnetic ordering in an fcc structure [51].

It should be pointed out that although the calculated Curie temperatures, using theoretical exchange coupling parameters within the Heisenberg model, agree reasonably well with experiment, it is still difficult to uniquely attribute the mechanism of exchange interactions in these compounds to the RKKY or superexchange mechanisms. The relative contribution from RKKY interaction varies considerably due to the change in metallicity across the monopnictides. For example, if the system is insulating, the RKKY interactions should vanish. Therefore, in addition to the RKKY exchange and superexchange contributions, other exchange coupling mechanisms are possible in the rare-earth monopnictides, such as higher order exchange interactions [37], direct exchange, and double exchange interactions. Actually, there is experimental evidence that direct exchange coupling could be responsible for the higher Curie temperature found in insulating GdN films [126].

5.4. Spin–orbit coupling

Spin–orbit coupling is important for correctly deriving the band structure and many other properties, e.g. magneto-crystalline anisotropy, of compounds containing heavier elements like rare-earths. For Gd ions, the spin–orbit term $\xi\sigma \cdot L$ (here σ and L are spin and orbital angular momentum operators, respectively) may be ignored since the 4f shells are exactly half occupied. For other rare-earth ions with non-zero total orbital angular momentum, the spin–orbit term may be significant. There are very few *ab initio* calculations on the rare-earth pnictides involving spin–orbit coupling. Duan *et al* studied the spin–orbit effect in ErAs [85], and Johannes and Pickett also considered this effect in their studies on EuN and EuP [91]. Leuenberger *et al* mentioned the presence of an important spin–orbit interaction in the final N p states of GdN [122].

Figure 16 presents the theoretical band structure of ErAs that takes into account both the Hubbard U term and the spin–orbit interaction. In this calculation, the inclusion of spin–orbit interaction is realized by a fully relativistic approach for the core electrons and a second variational method for the valence states [159]. In contrast to the LSDA $+ U$ result [84], the occupied 4f bands are split further due to spin–orbit coupling, leading to better agreement with experiments [85].

Spin–orbit coupling is at the heart of magneto-optical effects such as Kerr and Faraday polarization rotation. CeSb has been claimed to have a 90° Kerr rotation [160]. While the intrinsic value of the Kerr rotation of CeSb is still debated, agreement exists that CeSb has possibly the largest Kerr rotation, possibly the largest. A series of calculations of the magneto-optical properties of the rare-earth monopnictides reproduced experimental results with varying success [83, 92, 161].
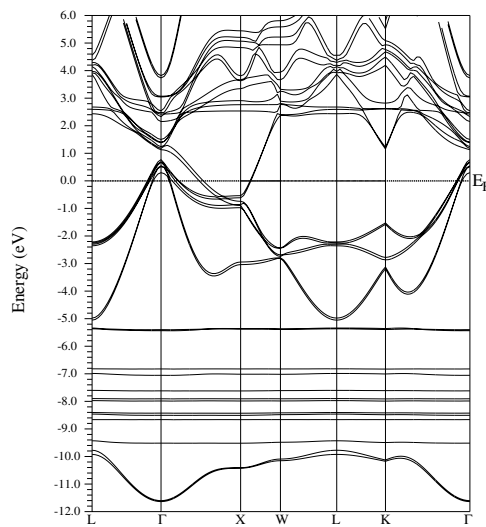
Figure 16. The calculated LSDA $+ U +$ SO band structure of bulk ErAs. In the spin–orbit calculation, spin-up and spin-down states are mixed (from [85]).

6. The future possibilities

While the rare-earth monopnictides have the simplest structure of the rare-earth compounds, substantive changes can be easily undertaken by altering the constituents. Actually, by mixing rare-earth pnictides in different ratios, we can tune the physical properties, for example T_c, carrier density, and resistance, of rare-earth pnictides to desired values [24, 38, 43, 47, 35, 164]. Impurity doping, and thus non-stoichiometry, also has a significant influence on the properties of rare-earth pnictides. These subjects are too complicated and are beyond the scope of this review. We just want to mention that there are many choices for improving the physical, magnetic and transport properties of rare-earth pnictides.

For binary rare-earth pnictide compounds, there are various types with different structures. For example, there are at least five structure types in the RX_2 phase, i.e. LaP_2, $NdAs_2$, $SmSb_2$, $HoSb_2$, $ZrSi_2$ [39]. Of particular interest, we mention the anti-Th_3P_4-type pnictides, which have attracted much interest recently [162, 163]. Some of the anti-Th_3P_4-type pnictides demonstrate very large values for T_c, as noted below. For ternary compounds, the situation is much more complicated [39]. Active experimental studies are being carried out on these systems [164–166].

6.1. Possible half-metallic antiferromagnets

In 1995, Van Leuken and de Groot proposed another type of half-metallic material, i.e. the half-metallic antiferromagnet [167]. This material is calculated to be 100% spin polarized at the Fermi surface but has zero net magnetization, and thus could be used as a tip material in spin-polarized scanning tunnelling microscopy. There are several theoretical predictions concerning the existence of the half-metallic antiferromagnet [167–170], but none of them has been confirmed experimentally.

Half-metallic antiferromagnets cannot be found with the simple pure rare-earth monopnictides, because the metallic spin channels are present in the two AFM sites of such materials. However, a mixed antiferromagnet such as EuO-GdN with Eu^{2+} and Gd^{3+}

aligned antiparallel, could have electronic structure suitable for half-metallic behaviour. If this prediction is verified, then this material would be a half-metallic antiferromagnet with the simplest structure (double fcc).

6.2. Enhancement of the transition temperatures and potential device applications

The rare-earth monopnictide compounds have generally rather low transition temperatures. GdN has the largest T_c (58–68 K), but it is still far below room temperature. How to improve the T_c in these compounds is of interest.

In 1971, Kuznietz reported the effect of anion substitution in GdN and UN [171]. It was found that carbon substitution can significantly improve T_c, while O substitution works the other way. An example is $GdN_{0.88}C_{0.12}$ ($Gd_4N_{3.5}C_{0.5}$ in [38]), whose T_c was reported to be as high as 190 K. This can be explained by the reduction of Gd–Gd distance, which may lead to an increase in 5d–5d overlap. Considering that Gd metal has somewhat higher T_c (293.2 K) [172], efforts in this direction are very promising. Wachter and Kaldis also confirmed this kind of effect of Gd–Gd distance [43]. Actually, [38] also reported that some other GdN derived alloys have T_c even higher than room temperature (340 K).

The other possibility for increasing T_c in the rare-earth pnictides is impurity doping. Magnetic impurities are helpful in assisting in the alignment of neighbouring magnetic moments and they strengthen the magnetic interactions or even change the RKKY interaction to a long-range ferromagnetic interaction, thus dramatically enhancing T_c. Examples can be found in [173], which reported that by adding a few per cent of magnetic ions such as Mn, the T_c of GaN or ZnO well exceeds room temperature. Again mentioning the experiments on GdN/Fe multilayers [127] in this context, it is worth noting that the Fe layers are found to be responsible for the long-range magnetic order in the GdN layer at temperatures largely above T_c.

In addition, we noticed that some rare-earth pnictides of the Th_3P_4 type (or its anti-type) have very high T_c values, even higher than that of Gd metal. For example, the T_c of Gd_4Bi_3 is 340 K [174], for Gd_4Sb_3 it is 260 K [175], and for Tb_4Bi_3 it is 200 K. The origin of these high T_cs needs further investigation.

Despite their low transition temperatures, applications for the rare-earth pnictides do exist. For example, ErAs has been used to study magneto-transport [51] and resonant tunnelling [176]; EuS has been used in hybrid spin filter devices [177, 178]. These materials are of special interest for using as barriers in magnetic tunnel junctions [179]. This is due to the exchange splitting of the conduction band which makes the barrier height spin dependent. Thus, given the exponential dependence of the tunnelling current on barrier height, a highly spin-polarized current is expected. In a series of spin-dependent tunnelling experiments, Moodera *et al* found a tunnelling spin polarization of approximately 80% in Al/EuS/M junctions, where M was Ag, Au, or Al [180]. Using a related Eu chalcogenide, EuSe, they were able to demonstrate essentially 100% spin polarization [181]. New hybrid devices utilizing the spin filtering properties of rare-earth monopnictides are expected in the near future.

7. Conclusions

After more than 40 years' efforts, stimulated first by the search for magnetic semiconductors and now by spintronics materials, we now have a better understanding of the electronic, magnetic and transport properties of rare-earth monopnictides.

Rare-earth monopnictides are generally semiconductors or semimetals. Despite their simple rock salt structure, they demonstrate various types of magnetic ordering generally with

low transition temperatures. Their electronic structures and magnetic properties are sensitive to temperature, pressure (strain) and impurity effects. The rare-earth 4f–5d interactions and the hybridizations between the rare-earth non-4f and pnictogen p states are responsible for many fascinating phenomena that occur in rare-earth monopnictides. In contrast to the rare-earth metals, both superexchange interaction and indirect RKKY-type interaction coexist in rare-earth monopnictides, and the former is dominant in heavy rare-earth monopnictides. It is possible that other exchange coupling mechanisms, such as direct exchange and double exchange, may also be found in rare-earth monopnictides.

We conclude that the high-polarization, nominally half-metallic, rare-earth monopnictides are most likely to be found in rare-earth nitrides or nitrogen-involved rare-earth alloys. This is because those nitrides are on the border between semiconductor and metal due to their anion sizes. Impurity doping, structural distortion, and lattice constraint effects have a significant influence on the electronic, magnetic and transport properties of rare-earth nitrides.

During the past several decades, various theoretical and experimental studies have helped to study the intriguing properties of these materials. Theoretically, much more powerful tools have been developed to solve the complicated yet fascinating many-body problems existing in these strongly correlated systems, such as SIC, LSDA + U, GWA and DMFT. With the fast increase in the computational power and the more mature massively parallel computing technology, there is more confidence we can have to deal with the necessary large scale calculations.

State-of-the-art crystal and film growth techniques make it possible now to obtain high quality samples to determine the electronic structure, the Fermi surfaces, and physical properties of these compounds. With improved samples, techniques like low energy electron-diffraction, scanning tunnelling microscopy, angle-resolved (inverse) photoemission, neutron-diffraction are proving to be more helpful in characterizing the geometric, electronic and magnetic structures of both thin films and crystals, particularly when combined with element specific XMCD experiments.

Still, there are many unresolved issues related to the half-metallicity in rare-earth monopnictides and many blanks that need to be filled in table 1. To address these issues or fill in the blanks, a close collaboration between experimentalists and theorists is absolutely necessary. Nevertheless, it takes a little imagination to conclude that we can expect further exciting results to emerge from the study of the electronic structure of rare-earth compounds.

Acknowledgments

References

[1] de Groot R A, Mueller F M, van Engen P G and Buschow K H J 1983 *Phys. Rev. Lett.* **50** 2024
[2] Wolf S A, Awschalom D D, Buhrman R A, Daughton J M, von Molnar S, Roukes M L, Chtchelkanova A Y and Treger D M 2001 *Science* **294** 1488
[3] Pickett W E and Moodera J S 2001 *Phys. Today* **54** (May) 39

[4]   Dowben P A and Skomski R 2004 *J. Appl. Phys.* **95** 7453
[5]   Dowben P A and Jenkins S J 2005 *Frontiers in Magnetic Materials* ed A Narlikar (Berlin: Springer) p 295
[6]   Chioncel L, Katsnelson M I, de Groot R A and Lichtenstein A I 2003 *Phys. Rev.* B **68** 144425
[7]   Irkhin V Y and Katsnelson M I 1985 *J. Phys. C: Solid State Phys.* **18** 4173
[8]   For a complete review, see the series: Gschneidner K A and Eyring L (ed) 1979 *Handbook on Physics and Chemistry of Rare Earth* (Amsterdam: North-Holland)
[9]   Dowben P A, McIlroy D N and Li D 1997 *Handbook on the Physics and Chemistry of Rare Earths* vol 24, ed K A Gschneidner and L Eyring (Amsterdam: North-Holland) chapter 159
[10] Cullity B D 1972 *Introduction to Magnetic Materials* (Reading, MA: Addison-Wesley) p 178
[11] Yakovkin I N, Komesu T and Dowben P A 2002 *Phys. Rev.* B **66** 035406
[12] Olson C G, Chase S J, Canfield P and Lynch D W 1998 *J. Electron Spectrsoc. Relat. Phenom.* **93** 175
[13] Andrews A B, Joyce J J, Arko A J, Thompson J D, Tang J, Lawrence J M and Hemminger J C 1995 *Phys. Rev.* B **51** R3277
[14] Guziewicz E, Durakiewicz T, Butterfield M T, Olson C G, Joyce J J, Arko A J, Sarrao J L, Moore D P and Morales L 2004 *Phys. Rev.* B **69** 045102
[15] Guziewicz E, Durakiewicz T, Olson C G, Joyce J J, Butterfield M T, Arko A J, Sarrao J L and Wojakowski A 2006 *Surf. Sci.* **600** 1632
[16] Guziewicz E, Durakiewicz T, Oppeneer P M, Joyce J J, Thompson J D, Olson C G, Butterfield M T, Wojakowski A, Moore D P and Arko A J 2006 *Phys. Rev.* B **73** 155119
[17] Anderson P W 1959 *Phys. Rev.* **115** 2
[18] Anderson P W 1978 *Rev. Mod. Phys.* **50** 191
[19] Van Vleck J H and Frank A 1929 *Phys. Rev.* **34** 1494
[20] Van Vleck J H 1978 *Rev. Mod. Phys.* **50** 181
[21] Sclar N 1962 *J. Appl. Phys.* **33** 2999
      Sclar N 1964 *J. Appl. Phys.* **35** 1534
[22] Child H R, Wilkinson M K, Cable J W, Koehler W C and Wollan E O 1963 *Phys. Rev.* **131** 922
[23] Trammell G T 1963 *Phys. Rev.* **131** 932 and references therein
[24] Holtzberg F, McGuire T R, Methfessel S and Suits J C 1964 *Phys. Rev. Lett.* **13** 18
      Holtzberg F, McGuire T R, Methfessel S and Suits J C 1964 *J. Appl. Phys.* **35** 1033
      Holtzberg F, McGuire T R, Methfessel S and Suits J C 1966 *J. Appl. Phys.* **37** 976
[25] Busch G 1967 *J. Appl. Phys.* **38** 1386 and references therein
[26] Brown R F, Lawson A W and Everett G E 1968 *Phys. Rev.* **172** 559
[27] McGuire T R, Gambino R J, Pickart S J and Alperin H A 1969 *J. Appl. Phys.* **40** 1009
[28] Birgeneau R J, Bucher E, Maita J P, Passell L and Turberfield K C 1973 *Phys. Rev.* B **8** 5345
[29] Narita A and Kasuya T 1985 *J. Magn. Magn. Mater.* **52** 373
[30] Takahashi H and Kasuya T 1985 *J. Phys. C: Solid State Phys.* **18** 2697
      Takahashi H and Kasuya T 1985 *J. Phys. C: Solid State Phys.* **18** 2709
[31] Hasegawa A and Yanase A 1977 *J. Phys. Soc. Japan* **42** 492
[32] Slater J C 1951 *Phys. Rev.* **81** 385
[33] Narita A 1988 *J. Phys. Soc. Japan* **57** 251
      Narita A 1988 *J. Phys. Soc. Japan* **57** 3961
[34] Xia J-B, Ren S-F and Chang Y-C 1991 *Phys. Rev.* B **43** 1692
[35] Petukhov A G, Lambrecht W R L and Segall B 1994 *Phys. Rev.* B **50** 7800
[36] Petukhov A G, Lambrecht W R L and Segall B 1996 *Phys. Rev.* B **53** 4324
[37] Kasuya T and Li D X 1997 *J. Magn. Magn. Mater.* **167** L1
[38] Rhyne J J and McGuire T R 1972 *IEEE Trans. Magn.* **8** 105
[39] Hulliger F 1979 *Handbook on the Physics and Chemistry of Rare Earths* vol 4, ed K A Gschneidner and L Eyring (Amsterdam: North-Holland) chapter 33, p 153
[40] Kaldis E 1974 *J. Cryst. Growth* **24/25** 53
[41] Güntherodt G, Kaldis E and Wachter P 1974 *Solid State Commun.* **15** 1435
[42] Kaldis E and Zurcher C 1974 *Helv. Phys. Acta* **47** 421
[43] Wachter P and Kaldis E 1980 *Solid State Commun.* **34** 241
[44] Ruderman M A and Kittel C 1954 *Phys. Rev.* **96** 99
[45] Kasuya T 1956 *Prog. Theor. Phys. (Kyoto)* **16** 45
[46] Yosida K 1957 *Phys. Rev.* **106** 893
[47] Wachter P, Kaldis E and Hauger R 1978 *Phys. Rev. Lett.* **40** 1404
[48] Wachter P 1978 *Phys. Rep.* **44** 159
[49] Urban P, Jansen K, Sperlich G and Davidov D 1978 *J. Phys. F: Met. Phys.* **8** 977

[50] Palmstrøm C J, Tabatabaie N and Allen S J 1988 *Appl. Phys. Lett.* **53** 2608
[51] Allen S J, Tabatabaie N, Palmstrøm C J, Hull G W, Sands T, DeRosa F, Gilchrist H L and Garrison K C 1989 *Phys. Rev. Lett.* **62** 2309
[52] Degiorgi L, Bacsa W and Wachter P 1990 *Phys. Rev.* B **42** 530
[53] Degiorgi L, Teraoka S, Compagnini G and Wachter P 1993 *Phys. Rev.* B **47** 5715
[54] Chattopadhyay T, Burlet P, Rossat-Mignod J, Bartholin H, Vettier C and Vogt O 1994 *Phys. Rev.* B **49** 15096
[55] Waldfried C, McIlroy D N, Li D, Pearson J, Bader S D and Dowben P A 1995 *Surf. Sci.* **341** L1072
[56] Xiao J Q and Chien C L 1996 *Phys. Rev. Lett.* **76** 1727
[57] Li D X, Haga Y, Shida H, Suzuki T, Koide T and Kido G 1996 *Phys. Rev.* B **53** 8473
[58] Li D X, Haga Y, Shida H, Suzuki T and Kwon Y S 1996 *Phys. Rev.* B **54** 10483
[59] Yamada H, Fukawa T, Muro T, Tanaka Y, Imada S, Suga S, Li D-X and Suzuki T 1996 *J. Phys. Soc. Japan* **65** 1000
[60] Li D X, Haga Y, Shida H, Suzuki T, Kwon Y S and Kido G 1997 *J. Phys.: Condens. Matter* **9** 10777
[61] Jones R O and Gunnarsson O 1989 *Rev. Mod. Phys.* **61** 689
[62] Perdew J P and Zunger A 1981 *Phys. Rev.* B **23** 5048 and references therein
[63] Cowan R D 1967 *Phys. Rev.* **163** 54
[64] Heaton R A, Harrison J G and Lin C C 1983 *Phys. Rev.* B **28** 5992
[65] Svane A and Gunnarsson O 1990 *Phys. Rev. Lett.* **65** 1148
[66] Svane A and Gunnarsson O 1988 *Phys. Rev.* B **37** 9919
[67] Strange P, Svane A, Temmerman W M, Szotek Z and Winter H 1999 *Nature* **399** 756
[68] Petit L, Svane A, Szotek Z and Temmerman W M 2003 *Science* **301** 498
[69] Svane A 1992 *Phys. Rev. Lett.* **68** 1900
[70] Aerts C M, Strange P, Horne M, Temmerman W M, Szotek Z and Svane A 2004 *Phys. Rev.* B **69** 045115
[71] Horne M, Strange P, Temmerman W M, Szotek Z, Svane A and Winter H 2004 *J. Phys.: Condens. Matter* **16** 5061
[72] Szotek Z, Temmerman W M, Svane A, Petit L, Strange P, Stocks G M, Ködderitzsch D, Hergert W and Winter H 2004 *J. Phys.: Condens. Matter* **16** S5587
[73] Svane A, Kanchana V, Vaitheeswaran G, Santi G, Temmerman W M, Szotek Z, Strange P and Petit L 2005 *Phys. Rev.* B **71** 045119
[74] Hubbard J 1963 *Proc. R. Soc.* A **276** 238
     Hubbard J 1964 *Proc. R. Soc.* A **277** 237
     Hubbard J 1964 *Proc. R. Soc.* A **281** 401
[75] Anisimov V I, Zaanen J and Andersen O K 1991 *Phys. Rev.* B **44** 943
[76] Anisimov V I, Solovyev I V, Korotin M A, Czyzyk M T and Sawatzky G A 1993 *Phys. Rev.* B **48** 16929
[77] Liechtenstein A I, Anisimov V I and Zaanen J 1995 *Phys. Rev.* B **52** R5467
[78] Anisimov V I, Aryasetiawan F and Lichtenstein A I 1997 *J. Phys.: Condens. Matter* **9** 767
[79] Anderson P W 1961 *Phys. Rev.* **124** 41
[80] Dudarev S L, Botton G A, Savrasov S Y, Humphreys C J and Sutton A P 1998 *Phys. Rev.* B **57** 1505
[81] Anisimov V I and Gunnarsson O 1991 *Phys. Rev.* B **43** 7570
[82] Slater J C 1960 *Quantum Theory of Atomic Structure* vol 1 (New York: McGraw-Hill)
[83] Liechtenstein A I, Antropov V P and Harmon B N 1994 *Phys. Rev.* B **49** 10770
[84] Komesu T, Jeong H-K, Choi J, Borca C N, Dowben P A, Petukhov A G, Schultz B D and Palmström C J 2003 *Phys. Rev.* B **67** 035104
[85] Duan C-G, Komesu T, Jeong H-K, Choi J, Borca C N, Yin W-G, Liu J, Mei W N, Dowben P A, Petukhov A G, Schultz B D and Palmstrøm C J 2004 *Surf. Rev. Lett.* **11** 531
[86] Blaha P, Schwarz K, Madsen G K H, Kvasnicka D and Luitz J 2001 *WIEN2k, An Augmented Plane Wave + Local Orbitals Program for Calculating Crystal Properties* (Karlheinz Schwarz, Techn. Universität Wien, Austria) ISBN 3-9501031-1-2
[87] Duan C-G, Sabiryanov R F, Liu J, Mei W N, Dowben P A and Hardy J R 2005 *J. Appl. Phys.* **97** 10A915
[88] Duan C-G, Sabiryanov R F, Liu J, Mei W N, Dowben P A and Hardy J R 2005 *Phys. Rev. Lett.* **94** 237201
     Duan C-G, Sabiryanov R F, Liu J, Mei W N, Dowben P A and Hardy J R 2006 *Phys. Rev. Lett.* **96** 139901
[89] Duan C-G, Sabiryanov R F, Mei W N, Jaswal S S, Dowben P A and Tsymbal E Y 2006 *Appl. Phys. Lett.* **88** 182505
[90] Anderson P W 1950 *Phys. Rev.* **79** 350
     Anderson P W 1959 *Phys. Rev.* **115** 2
[91] Johannes M D and Pickett W E 2005 *Phys. Rev.* B **72** 195116
[92] Ghosh D B, De M and De S K 2005 *Phys. Rev.* B **72** 045140
[93] Larson P and Lambrecht W R L 2006 *Phys. Rev.* B **74** 085108

[94] Kohn W and Sham L J 1965 *Phys. Rev.* **140** A1133
[95] Landau L D 1957 *Sov. Phys.—JETP* **3** 920
       Landau L D 1957 *Sov. Phys.—JETP* **5** 101
       Landau L D 1959 *Sov. Phys.—JETP* **35** 70
[96] Aryasetiawan F and Gunnarsson O 1998 *Rep. Prog. Phys.* **61** 237
[97] Hedin L 1965 *Phys. Rev.* **139** A796
[98] Pines D and Bohm D 1952 *Phys. Rev.* **85** 338
[99] Hybertsen M S and Louie S G 1985 *Phys. Rev. Lett.* **55** 1418
       Hybertsen M S and Louie S G 1988 *Phys. Rev.* B **37** 2733
[100] Godby R W, Schlüter M and Sham L J 1986 *Phys. Rev. Lett.* **56** 2415
[101] Onida G, Reining L and Rubio A 2002 *Rev. Mod. Phys.* **74** 601
[102] van Schilfgaarde M, Kotani T and Faleev S 2006 *Phys. Rev. Lett.* **96** 226402
[103] Lambrecht W R L 2000 *Phys. Rev.* B **62** 13538
[104] For a recent review, see Kotliar G, Savrasov S Y, Haule K, Oudovenko V S, Parcollet O and Marianetti C A 2006
       Rev. Mod. Phys. **78** 865
[105] Metzner W and Vollhardt D 1989 *Phys. Rev. Lett.* **62** 324
[106] Georges A, Kotliar G, Krauth W and Rozenberg M J 1996 *Rev. Mod. Phys.* **68** 13
[107] Anisimov V I, Poteryaev A I, Korotin M A, Anokhin A O and Kotliar G 1997 *J. Phys.: Condens. Matter* **9** 7359
[108] Chitra R and Kotliar G 2000 *Phys. Rev.* B **62** 12715
[109] Lægsgaard J and Svane A 1998 *Phys. Rev.* B **58** 12817
[110] Sakai O, Shimizu Y and Kaneta Y 2005 *J. Phys. Soc. Japan* **74** 2517
[111] Kalvoda S, Dolg M, Flad H-J, Fulde P and Stoll H 1998 *Phys. Rev.* B **57** 2127
[112] Santos C, Nolting W and Eyert V 2004 *Phys. Rev.* B **69** 214412
[113] Sharma A and Nolting W 2006 *J. Phys.: Condens. Matter* **18** 7337
[114] Bhattacharjee S and Jaya S M 2006 *Eur. Phys. J.* B **49** 305
[115] Landrum G A, Dronskowski R, Niewa R and DiSalvo F J 1999 *Chem. Eur. J.* **5** 515
[116] Marzari N and Vanderbilt D 1997 *Phys. Rev.* B **56** 12847
[117] Stengel M and Spaldin N A 2006 *Phys. Rev.* B **73** 075121
[118] Koyama K, Yoshida M, Nojiri H, Sakon T, Li D X, Suzuki T and Motokawa M 2000 *J. Phys. Soc. Japan*
       69 1521
[119] Koyama K, Yoshida M, Li D X and Motokawa M 2001 *J. Phys. Soc. Japan* **70** 2774
[120] Tomimatsu T, Koyama K, Yoshida M, Li D X and Motokawa M 2003 *Phys. Rev.* B **67** 014406
[121] Nakanishi Y, Sakon T, Motokawa M, Ozawa M and Suzuki T 2004 *Phys. Rev.* B **69** 024412
[122] Leuenberger F, Parge A, Felsch W, Fauth K and Hessler M 2005 *Phys. Rev.* B **72** 014427
[123] Oliver M R, Kafalas J A, Dimmock J O and Reed T B 1970 *Phys. Rev. Lett.* **24** 1064
[124] Shapira Y, Foner S, Aggarwal R L and Reed T B 1973 *Phys. Rev.* B **8** 2316
[125] Leuenberger F, Parge A, Felsch W, Baudelet F, Giorgetti C, Dartyge E and Wilhelm F 2006 *Phys. Rev.* B
       73 214430
[126] Granville S, Ruck B J, Budde F, Koo A, Pringle D J, Kuchler F, Preston A R H, Housden D H, Lund N, Bittar A,
       Williams G V M and Trodahl H J 2006 *Phys. Rev.* B **73** 235335
[127] Leuenberger F, Parge A, Felsch W, Neisius T and Mathon O 2006 *J. Appl. Phys.* **100** 033905
[128] Olcese G L 1979 *J. Phys. F: Met. Phys.* **9** 569
[129] Smart J S 1966 *Effective Field Theories of Magnetism* (Philadelphia, PA: Saunders) pp 76–7
[130] Ono S, Nomura K and Hayakawa H 1972 *J. Less Common Met.* **38** 119
[131] Iandelli A and Botti E 1976 *Atti Accad. Naz. Lincei Cl. Sci. Fis. Mat. Nat. Rend.* **254** 498
[132] Leger J M, Ravot D and Rossat-Mignod J 1984 *J. Phys. C: Solid State Phys.* **17** 4935
[133] Nomura K, Hayakawa H and Ono S 1977 *J. Less Common Met.* **52** 259
[134] Schoenes J and Reim W 1985 *J. Less Common Met.* **112** 19
[135] Ettmayer P, Waldhart J and Vendl A 1979 *Mon. Chem.* **110** 1109
[136] Jacobs H and Fink U 1978 *Z. Anorg. Allg. Chem.* **438** 151
[137] Mironov K E and Brygalina G P 1974 *Izv. Akad. Nauk SSSR Neorg. Mater.* **10** 787
[138] Bommeli F, Degiorgi L and Wachter P 1995 *J. Magn. Magn. Mater.* **140** 1159
[139] Li D X, Oyamada A, Hashi K, Haga Y, Matsumura T, Shida H, Suzuki T, Kasuya T, Dönni A and
       Hulliger F 1995 *J. Magn. Magn. Mater.* **140** 1169
[140] Klemm W and Winkelmann G 1956 *Z. Anorg. Allg. Chem.* **288** 87
[141] Iandelli A 1964 *Atti Accad. Naz. Lincei Cl. Sci. Fis. Mat. Nat. Rend.* **37** 160
[142] Harmon B N, Antropov V P, Liechtenstein A I, Solovyev I V and Anisimov V I 1995 *J. Phys. Chem. Solids*
       56 1521

[143] Shick A B, Liechtenstein A I and Pickett W E 1999 *Phys. Rev.* B **60** 10763
[144] Kurz Ph, Bihlmayer G and Blügel S 2002 *J. Phys.: Condens. Matter* **14** 6353
[145] Steglich F, Rauchschwalbe U, Gottwick U, Mayer H M, Sparn G, Grewe N, Poppe U and Franse J J M 1985
        J. Appl. Phys. **57** 3054
[146] Rice T M and Ueda K 1985 *Phys. Rev. Lett.* **55** 995
[147] Monnier R, Rhyner J, Rice T M and Koelling D D 1985 *Phys. Rev.* B **31** 5554
[148] Ashcroft N W and Mermin N D 1976 *Solid State Physics* (New York: Holt, Rinehart, and Winston) p 652
[149] Galanakis I, Dederichs P H and Papanikolaou N 2002 *Phys. Rev.* B **66** 174429
[150] Waldfried C, McAvoy T, Welipitiya D, Komesu T, Dowben P A and Vescovo E 1998 *Phys. Rev.* B **58** 7434
[151] Komesu T, Waldfried C and Dowben P A 1999 *Phys. Lett.* A **256** 81
[152] Oleinik I I, Tsymbal E Y and Pettifor D G 2002 *Phys. Rev.* B **65** R020401
[153] Velev J, Belashchenko K D, Stewart D, van Schilfgaarde M, Jaswal S S and Tsymbal E Y 2005 *Phys. Rev. Lett.*
        95 216601
[154] Duan C-G, Jaswal S S and Tsymbal E Y 2006 *Phys. Rev. Lett.* **97** 047201
[155] Dowben P A 2000 *Surf. Sci. Rep.* **40** 151
[156] Falicov L M and Kimball J C 1969 *Phys. Rev. Lett.* **22** 997
[157] Kreissl M and Nolting W 2005 *Phys. Rev.* B **72** 245117
[158] Harrison W A 1980 *Electronic Structure and the Properties of Solids* (San Francisco, CA: Freeman) pp 451,
        481 and 505
[159] Singh D J 1994 *Planewaves, Pseudopotentials and the LAPW Method* (Boston, MA: Kluwer Academic) p 86
[160] Pittini R, Schoenes J, Vogt O and Wachter P 1996 *Phys. Rev. Lett.* **77** 944
[161] Ghosh D B, De M and De S K 2003 *Phys. Rev.* B **67** 035118
[162] Szade J and Drzyzga M 2000 *J. Alloys Compounds* **299** 72
[163] Drzyzga M, Szade J, Deniszczyk J and Michalecki T 2003 *J. Phys.: Condens. Matter* **15** 3701
[164] Weber F, Cosceev A, Nateprov A, Pfleiderer C, Faisst A, Uhlarz M and Lohneysen H V 2005 *Physica* B **359** 226
[165] Mozharivskyj Y and Franzen H F 2000 *J. Solid State Chem.* **152** 478
[166] Schneemeyer L F, van Dover R B and Gyorgy E M 1987 *J. Appl. Phys.* **61** 3543
[167] van Leuken H and de Groot R A 1995 *Phys. Rev. Lett.* **74** 1171
[168] Pickett W E 1998 *Phys. Rev.* B **57** 10613
[169] Min B I, Park M S and Park J H 2004 *J. Phys.: Condens. Matter* **16** S5509
[170] Akai H and Ogura M 2006 *Phys. Rev. Lett.* **97** 026401
[171] Kuznietz M 1971 *J. Appl. Phys.* **42** 1470
[172] Nigh H E, Legvold S and Spedding F H 1963 *Phys. Rev.* **132** 1092
[173] Coey J M, Venkatesan M and Fitzgerald C B 2005 *Nat. Mater.* **4** 173
[174] Methfessel S and Kneller E 1963 *Appl. Phys. Lett.* **2** 115
[175] Holtzberg F, McGuire T R, Methfessel S and Suits J C 1964 *J. Appl. Phys.* **35** 1033
[176] Brehmer D E, Zhang K, Schwarz C J, Chau S P and Allen S J 1995 *Appl. Phys. Lett.* **67** 1268
[177] LeClair P, Ha J K, Swagten H J M, Kohlhepp J T, van de Vin C H and de Jonge W J M 2002 *Appl. Phys. Lett.*
        80 625
[178] Filip A T, LeClair P, Smits C J P, Kohlhepp J T, Swagten H J M, Koopmans B and de Jonge W J M 2002 *Appl.
        Phys. Lett.* **81** 1815
[179] Tsymbal E Y, Mryasov O and LeClair P R 2003 *J. Phys.: Condens. Matter* **15** R109
[180] Moodera J S, Hao X, Gibson G A and Meservey R 1988 *Phys. Rev. Lett.* **61** 637
[181] Moodera J S, Meservey R and Hao X 1993 *Phys. Rev. Lett.* **70** 853